Functional specialization of macaque premotor F5 subfields with respect to hand and mouth movements: A comparison of task and resting-state fMRI

S. Sharma [a,b], D. Mantini [c,d], W. Vanduffel [a,b,e,f], K. Nelissen [a,b,*]

[a] Laboratory for Neuro- & Psychophysiology, Department of Neurosciences, KU Leuven, 3000, Leuven, Belgium
[b] Leuven Brain Institute, KU Leuven, 3000, Leuven, Belgium
[c] Movement Control & Neuroplasticity Research Group, KU Leuven, Leuven, Belgium
[d] Functional Neuroimaging Laboratory, Fondazione Ospedale San Camillo - IRCCS, Venezia, Italy
[e] Athinoula A. Martinos Center for Biomedical Imaging, Massachusetts General Hospital, Charlestown, MA, 02129, USA
[f] Department of Radiology, Harvard Medical School, Boston, MA, 02115, USA

ARTICLE INFO

ABSTRACT

Based on architectonic, tract-tracing or functional criteria, the rostral portion of ventral premotor cortex in the macaque monkey, also termed area F5, has been divided into several subfields. Cytoarchitectonical investigations suggest the existence of three subfields, F5c (convexity), F5p (posterior) and F5a (anterior). Electrophysiological investigations have suggested a gradual dorso-ventral transition from hand- to mouth-dominated motor fields, with F5p and ventral F5c strictly related to hand movements and mouth movements, respectively. The involvement of F5a in this respect, however, has received much less attention. Recently, data-driven resting-state fMRI approaches have also been used to examine the presence of distinct functional fields in macaque ventral premotor cortex. Although these studies have suggested several functional clusters in/near macaque F5, so far the parcellation schemes derived from these clustering methods do not completely retrieve the same level of F5 specialization as suggested by aforementioned invasive techniques. Here, using seed-based resting-state fMRI analyses, we examined the functional connectivity of different F5 seeds with key regions of the hand and face/mouth parieto-frontal-insular motor networks. In addition, we trained monkeys to perform either hand grasping or ingestive mouth movements in the scanner in order to compare resting-state with task-derived functional hand and mouth motor networks. In line with previous single-cell investigations, task-fMRI suggests involvement of F5p, dorsal F5c and F5a in the execution of hand grasping movements, while non-communicative mouth movements yielded particularly pronounced responses in ventral F5c. Corroborating with anatomical tracing data of macaque F5 subfields, seed-based resting-state fMRI suggests a transition from predominant functional correlations with the hand-motor network in F5p to mostly mouth-motor network functional correlations in ventral F5c. Dorsal F5c yielded robust functional correlations with both hand- and mouth-motor networks. In addition, the deepest part of the fundus of the inferior arcuate, corresponding to area 44, displayed a strikingly different functional connectivity profile compared to neighboring F5a, suggesting a different functional specialization for these two neighboring regions.

1. Introduction

The anatomical and functional organization of the rostral portion of the ventral premotor cortex in the macaque monkey, also termed F5 (Gentilucci et al., 1988; Matelli et al., 1985; Rizzolatti and Luppino, 2001), has been the focus of many investigations over the past decades. Recent cytoarchitectonic studies (Belmalih et al., 2009) have shown that this portion of agranular cortex can be subdivided into three sectors: F5p

(posterior) and F5a (anterior) at different anterior-posterior levels within the posterior bank of the inferior arcuate sulcus, and F5c (convexity) located on the adjacent convexity of the postarcuate cortex. If, and how strictly, this tripartite F5 architectonic organization may reflect a difference in functional specialization is less clear.

Electrophysiological and neuroimaging studies in macaques have shown that, from a functional motor point of view, neurons in F5p and the dorsal portion of F5c exhibit responses during skilled manual motor

---

acts such as object grasping or manipulation with the hand (di Pellegrino et al., 1992; Fiave et al., 2018; Fluet et al., 2010; Gallese et al., 1996; Gentilucci et al., 1988; Kraskov et al., 2009; Murata et al., 1997; Nelissen et al., 2018; Nelissen and Vanduffel, 2011; Raos et al., 2006; Sharma et al., 2018). A subset of the grasping-related motor neurons in F5p and dorsal F5c (Bonini et al., 2014) also discharge selectively to the visual presentation of graspable 3D objects, and it has been suggested that these so-called canonical neurons play a crucial role in transforming object properties such as size, shape and orientation into appropriate potential motor programs for hand-object interactions (Borra et al., 2017; Jeannerod et al., 1995).

The possible functional role of the most anterior F5 sector in the posterior bank of the arcuate, F5a, has received considerably less attention than have F5p and F5c. Non-invasive neuroimaging investigations have suggested both 3D shape (Joly et al., 2009) and grasping-related (Nelissen and Vanduffel, 2011) responses in macaque F5a. A subsequent single-cell investigation of this anterior arcuate region confirmed the presence of grasping-related motor neurons and showed that a majority of F5a neurons displayed selectivity for disparity-defined curved surfaces (Theys et al., 2012). Moreover, many of these 3D shape selective neurons were particularly active during visually guided grasping (as opposed to grasping in the dark), suggesting this area also plays a specific role in the visual analysis of 3D object properties related to object grasping (Schaffelhofer and Scherberger, 2016; Theys et al., 2012).

Despite the wealth of studies investigating the functional properties of premotor F5 in relation to hand motor acts, relatively few studies have investigated mouth motor responses in F5 (for recent review, see Ferrari et al., 2017). Earlier electrophysiology studies reported mouth-related responses in F5c, particularly during grasping with the mouth or biting/chewing food (Gallese et al., 1996; Gentilucci et al., 1988; Kurata and Tanji, 1986; Rizzolatti et al., 1988). Ferrari et al. (2003) and later Maranesi et al. (2012) expanded on this view and showed responses in ventral F5c to simpler mouth-related actions such as sucking juice from a syringe or licking involving tongue protrusion and retraction. Moreover, Ferrari et al. (2003) showed that some neurons in ventral F5c also responded during intransitive communicative face gestures such as lip smacking. A more recent study suggests that some neurons in this sector of F5c, besides responding during mouth-related motor responses such as licking, sucking, biting and chewing, also responded during conditioned vocalizations (Coudé et al., 2011). So far, orofacial responses have not been systematically investigated in F5a. However, in neighboring dysgranular area 44 located in the fundus of the inferior arcuate sulcus and in adjacent prefrontal area 45, orofacial responses related to tongue and jaw movements or neural responses related to vocalizations have been described (Hage and Nieder, 2015; Petrides et al., 2005).

Besides functional task-related and anatomical investigations of F5, recent studies have also used data-driven resting-state fMRI analyses in an attempt to parcellate the ventral premotor cortex and adjacent fields in the monkey. Although these resting-state fMRI studies suggested several distinct functional clusters in/near ventral premotor cortex, the particular specialization of F5 subfields as suggested by either architectonics (Belmalih et al., 2009) or functional criteria (Ferrari et al., 2017) is not completely retrieved from these data-driven resting-state clustering analyses. For instance, Goulas and co-authors (2017) suggest the existence of an F5c cluster on the postarcuate convexity, flanked posteriorly by a large F4 cluster, and anteriorly by a 44 cluster in the arcuate sulcus. Using similar data-driven methods, more recently Vijayakumar et al. (2018) on the other hand suggested the existence of one large F5 cluster, flanked dorsally by an F4 cluster and anteriorly by a large area 44 cluster.

Here, in order to examine the functional specialization of all F5 subfields with respect to hand and simple non-communicative mouth movements, we examined seed-based resting-state functional correlations of seeds placed in the different F5 subregions, in a group of eight rhesus monkeys. Besides seed-to-brain, we examined in detail F5 seed correlations with other seeds placed in different portions of the hand and mouth motor networks. In addition, two of these eight monkeys were

also trained to perform hand grasping or ingestive mouth movements (licking and tongue-protrusion movements) in the scanner, in order to compare functional networks derived from resting-state correlations with those networks observed during active motor tasks.

2. Materials and methods

2.1. Subjects

In total, eight macaque monkeys (monkeys M1 – M8, Macaca mulatta, 6 male, 2 female, 5–8 kgs) participated in the resting-state experiments. Two of them (male, M1 and M2, 6–7 kgs) also participated in the task-based fMRI experiments to localize regions responding to hand and mouth movements. Animal care and experimental procedures were approved by the animal ethical committee of KU Leuven and followed national and European guidelines.

### 2.2. Resting-state fMRI experiment

For the awake resting-state fMRI experiments, the monkeys simply had to fixate on a red dot in the center of the screen while getting juice rewards (Mantini et al., 2011). A single resting-state fMRI run lasted for 300 vol(umes), or 10 min.

2.3. Hand movement localizer

The grasping motor task used here to localize hand movement regions comprises the same task and data presented previously (Sharma et al., 2018) and follows similar procedures as Nelissen and Vanduffel (2011); Nelissen et al. (2018); Fiave et al. (2018). Before scanning, the monkeys were trained to sit in a sphinx position in a plastic chair facing a display screen in a mock scanner. During training, subjects had to maintain fixation within a $2 \times 2°$ window centered on a red dot ($0.35 \times 0.35°$) while being rewarded with fruit juice. Eye position was monitored at 120 Hz through pupil position and corneal reflection (ISCAN, Inc.). Once the fixation performance reached 85% or more, they were trained to grasp, spheres of 16, 23 or 40 mm radius with the right hand and subsequently scanned. In the grasping motor task, the fixation baseline comprised passively fixating on the red dot while maintaining the hand in the start position. For a grasping trial to begin, the monkey had to place his right hand in the start position while fixating on a green cue ($0.35 \times 0.35°$) displayed on the center of the screen. After a random fixation time of 500–1500 ms the green cue turned blue, signaling the monkey to reach forward and grasp the object placed in front of him (Fig. 1A). After grasping the object, the monkey received a juice reward for lifting the object 5 mm and holding it in that position for 500 ms. Once a trial was executed correctly, a new trial started with the presentation of the green cue as soon as the monkey's hand returned to the start position. Optic fibers were placed at the start and end positions and at two other positions along the reaching trajectory to track the location of hand and arm and to monitor the timing of the motor task execution. As a control for the grasping task, the monkeys had to perform a reach-only task during which there was an empty slot in front of them instead of an object, whereby they simply had to place their hand on the disk (palm down) for 500 ms to get a juice reward. The reach-only task contained exactly the same visual cues (green target turning blue) as for the grasping task. The motor tasks took place in the dark in the scanner to avoid responses due to visual feedback from the hand and arm or the object. Besides alternating between blocks of the two motor tasks, within the same runs, the monkeys were also required to keep the right hand in the start position while simply fixating a red fixation target in order to receive a juice reward (during fixation baseline blocks).

2.4. Mouth movement (taste) localizer

During this task (Fig. 1B), the monkeys were required to maintain
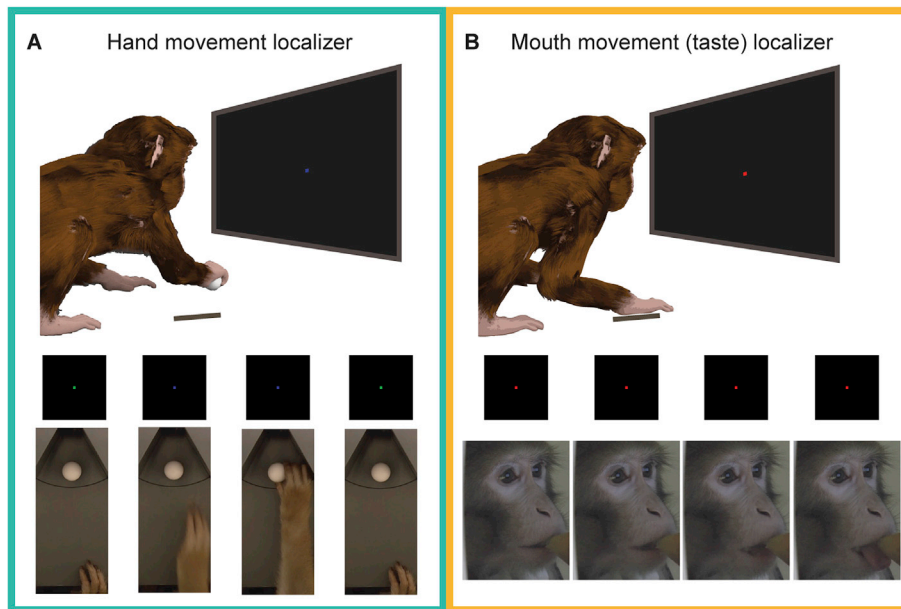
Fig. 1. Hand and mouth movement fMRI localizer tasks. **A**. Monkeys were trained to performed reach-and-grasp movements in the dark in the scanner, while being cued on a screen placed in front of them (see methods). **B**. In addition, the same monkeys were also scanned during a fixation task, during which they received random blocks of differently flavored liquids. Monkeys made significantly more licking and jaw movements when receiving the sweet liquid compared to receiving artificial saliva (see methods).

fixation on a red dot in the center of the screen (the same task as the fixation baseline in the hand movement localizer). The monkeys received randomly, in a blocked fashion, differently flavored rewards for keeping fixation. The different flavors included sweet (0.3 M sucrose in distilled water), sour (0.01 M citric acid in distilled water), salt (0.1 M Sodium Chloride in distilled water), bitter (0.0005 M quinine hydrochloride dehydrate in distilled water) or artificial saliva (potassium chloride 1.25 mM + sodium bicarbonate 0.125 mM in distilled water). Each block of a particular taste (30 s) was followed by a block of 10 s of distilled water to rinse out the taste of the previous condition. The artificial saliva condition was used as the baseline. During training sessions, we noticed that monkeys made substantial licking mouth movements, which was particularly pronounced when receiving the sweet liquid (compared to artificial saliva). We quantified this by recording videos of the monkeys' facial movements while they received the different liquids. Motion energy (optic flow) analysis of these videos confirmed that there were significantly more mouth movements when monkeys received sweet as opposed to artificial saliva rewards (monkey M1: $t = 6.87$; $p < 10^{-11}$; monkey M2: $t = 11$; $p < 10^{-25}$). Therefore, in order to visualize the brain regions responding during ingestive mouth movements, we contrasted ingesting the sweet-flavored liquid versus artificial saliva.

2.5. fMRI data acquisition

Data were acquired in a Siemens 3T full body scanner (TIM Trio or MAGNETOM Prisma[fit]) using a gradient-echo T2*-weighted echo-planar imaging sequence of 40 horizontal slices (hand movement localizer; resting-state experiments; TR = 2s, TE = 17 ms, flip angle = 90°, 1.25 mm isotropic) or 42 horizontal slices (mouth movement localizer; TR = 2s, TE = 17 ms, flip angle = 90°, 1.25 × 1.25 × 1.2 mm). An in-house designed and manufactured eight-channel phased array coil, and a saddle shaped, radial transmit-only surface coil was used for data acquisition (Kolster et al., 2009). Before each scanning session, an iron contrast agent (Molday ION, BioPAL in Monkey M1-M4 and MION; Sinerem, Laboratoire Guerbet in Monkey M5-M8) was injected intravenously (6–12 mg/kg) in order to improve signal-to-noise ratio (Vanduffel et al., 2001). A typical dose of contrast agent was 12 mg/kg, in case the same subject was scanned on consecutive days, this dose was gradually lowered to 6 mg/kg in order to maintain the optimal attenuation of MR signal by 50% (Mandeville et al., 1999; Vanduffel et al., 2001).

2.6. Experimental design of resting-state and task fMRI experiments

Awake, resting-state fMRI experiments consisted of runs of 300 vol(umes) or 10 min. For the resting-state fMRI data, we removed runs with substantial artifacts. Such runs were identified first by calculating the average correlation across voxel time-series. Those runs with a value below or above two times the median across runs were considered artifactual. Furthermore, runs with a fixation performance below 85% were excluded from further analysis (Mantini et al., 2011). This resulted in 18 runs from monkey M1, 19 runs from monkey M2, 17 runs from monkey M3, 19 runs from monkey M4, 18 runs from monkey M5, 14 runs from monkey M6, 15 runs from monkey M7 and 19 runs from monkey M8.

The hand movement localizer consisted of a block design with blocks of reach-grasp/reach-only execution, each followed by an equally long fixation-only block. For monkey M1, a run consisted of four start volumes followed by a sequence of blocks of grasping 16 mm sphere –fix only – grasping 40 mm sphere – fix only – grasping 23 mm sphere – fix only – reach – fix only – fixation baseline – fix only. In each of these blocks, 15 vol (30s duration) were acquired and the sequence of blocks was repeated once in the same run, resulting in total run of 304 volumes. The same design was used, but with a different object order (23 mm, 16 mm, and 40 mm spheres) for monkey M2. One run was excluded from monkey M2 due to poor performance, resulting in 12 runs from monkey M1 and 10 runs from monkey M2, which were combined for a fixed-effects group analysis. The hand-grasping fMRI data are those presented previously in Sharma et al. (2018).

The mouth movement (taste) localizer consisted also of a block design with four start volumes followed by blocks of either sweet, sour, salt, bitter or artificial saliva (each lasting for 15 vol or 30s). Each of these blocks was followed by a 10 s (5 vol) block of distilled water, resulting in a run of 204 volumes. The order of conditions (4 flavors and artificial saliva) was repeated once in a run and randomized across runs. FMRI fixed-effects group data analysis consisted of 20 runs (10 runs from monkey M1 and 10 runs from monkey M2).

2.7. Motion energy analysis

For both monkeys M1 and M2, mouth movements during ingestion of sweet liquid or artificial saliva were quantified by calculating the motion energy in the recorded videos (16 s, 400 frames). Motion energy was

calculated in a rectangular area centered on the mouth using the optic flow function (Horn-Schunck method) in Matlab. Statistical significance was assessed using two-tailed t tests between total motion energy in videos depicting monkeys receiving either the sweet liquid or the artificial saliva.

2.8. Data preprocessing

Data were preprocessed using statistical parametric mapping (SPM12) and JIP software (https://www.nitrc.org/projects/jip). Motion correction was performed by spatial realignment of all the functional images to the first image of the first run. Rigid and non-rigid co-registration of these realigned images to a template anatomy (monkey M12; Ekstrom et al., 2008; Nelissen and Vanduffel, 2011) was subsequently performed using JIP software. After co-registration, the images, now resliced to 1 mm isotropic voxel size, were smoothed with a 1.5 mm Gaussian kernel.

2.9. Resting-state fMRI analysis

2.9.1. Seed selection
In total, 25 different seeds (spheres of 2 mm radius, Mantini et al., 2011) were defined for either seed-to-brain or seed-to-seed functional correlation analyses. In addition to seeds in different sectors of F5 premotor cortex, we also defined seeds in typical hand-related or mouth-related areas, based upon anatomical landmarks and previous anatomical and functional studies (see below). Our functional MRI grasping and mouth movement localizers were used to verify that these additional seeds (10 mouth-related and 9 hand-related seeds) were indeed located in/near functionally responsive hand or mouth movement related regions. We investigated only seeds in the left hemisphere since monkeys performed the grasping task with the right hand only and therefore hand grasping-related fMRI motor activations were biased to the contralateral (left) hemisphere, as observed in previous monkey fMRI grasping investigations (Fiave et al., 2018; Nelissen et al., 2018; Nelissen and Vanduffel, 2011; Sharma et al., 2018).

2.9.2. Premotor F5 seeds
Guided by anatomical landmarks and previous anatomical and functional F5 studies (Belmalih et al., 2009; Fiave et al., 2018; Gerbella et al., 2011; Maranesi et al., 2012; Nelissen et al., 2005; Nelissen et al., 2018; Nelissen and Vanduffel, 2011), we defined four seeds in ventral premotor F5. These corresponded to the dorsal and ventral portions of F5c in the convexity of the postarcuate cortex, in addition to F5p and F5a, respectively, in the posterior and anterior portion of the posterior bank of the inferior arcuate sulcus. In addition to the F5a seed, two additional seeds were defined in more anterior and medial locations to explore the full extent of functional connectivity of the posterior bank and fundus of the arcuate sulcus, where dysgranular area 44 has been described (Caminiti et al., 2017; Frey et al., 2014; Neubert et al., 2014; Palomero-Gallagher and Zilles, 2018; Petrides et al., 2005). One of these two seeds corresponds respectively to the central part of the fundus of the inferior arcuate sulcus and is referred to as area 44 seed. The second seed is located in the most antero-ventral portion of the fundus towards the location of GrFO (Gerbella et al., 2016) and hence is referred to as 44/GrFO seed.

2.9.3. Additional hand-related seeds
Based upon anatomical landmarks and previous anatomical and functional studies, we defined a seed in the hand region of primary motor cortex F1 (Fiave et al., 2018; Nelissen et al., 2018; Nelissen and Vanduffel, 2011; Rizzolatti and Luppino, 2001). More anterior to this seed, another seed was defined in the caudal sector of the ventral premotor cortex. This location corresponds to the dorsal portion of F4, where the forelimb is represented and grasping responses have been observed (Maranesi et al., 2012; Nelissen and Vanduffel, 2011; Takahashi et al.,

2017). Posterior to F1, a seed was defined in the hand representation of somatosensory S1 (Sharma et al., 2018). In parietal cortex, four more hand-related seeds were defined: area PFG on the inferior parietal convexity (Gregoriou et al., 2006; Nelissen and Vanduffel, 2011; Rozzi et al., 2008), area AIP in the anterior portion of the lower bank of the intraparietal sulcus (Durand et al., 2007; Murata et al., 2000; Nelissen and Vanduffel, 2011), area PEip in the anterior portion of the upper bank of the intraparietal sulcus (Gardner, 2017; Matelli et al., 1998; Nelissen and Vanduffel, 2011) and area PE in the postcentral convexity (Gharbawie et al., 2011; Nelissen and Vanduffel, 2011; Squatrito et al., 2001). The AIP seed was placed in the most anterior portion of this region, given the well known motor to visual gradient along the anterior-posterior axis of this region (Nelissen and Vanduffel, 2011; Premereur et al., 2015). We defined another seed on the upper bank of the lateral sulcus, corresponding to the hand portion of the secondary somatosensory cortex S2 (Sharma et al., 2018) and a final hand-related seed in the dorso-posterior insula, where responses during active grasping movements have been described (Ishida et al., 2013; Sharma et al., 2018).

2.9.4. Additional mouth-related seeds
Similar to the hand-related seeds, based upon anatomical landmarks and previous anatomical and functional studies, we also defined several seeds in regions previously shown to respond during mouth movements. These included a seed in the lateral (or ventral) sector of F1 (Huang et al., 1988; Murray and Sessle, 1992), located 5 mm ventral to the hand seed of F1. Anterior to the mouth F1 seed, another seed was defined in the ventral portion of premotor F4, were orofacial movements are represented (Kurata, 2018; Maranesi et al., 2012). Posterior to F1, a seed was defined in the mouth representation of lateral S1 (Nelson et al., 1980; Qi et al., 2008), 5 mm ventral to the hand seed in S1. In parietal cortex, a seed was defined in area PF, where orofacial movements are represented (Ferrari et al., 2017; Rozzi et al., 2008). At the crown of the upper bank of the lateral sulcus, 6 mm lateral to the hand S2 seed, we defined a seed in the somatosensory mouth field of S2 (Krubitzer et al., 1995). Based upon previously described ingestive behavior during microstimulation in this sector in macaques (Jezzini et al., 2012), a mouth-related seed was also defined in the dorsal sector of the anterior insula. Three additional seeds were defined in the frontal operculum, corresponding to the dorsal opercular area DO (Belmalih et al., 2009; Gerbella et al., 2016), area PrCO (Belmalih et al., 2009) and area GrFO (Gerbella et al., 2016). Finally, a seed was placed in the anterior insula and adjacent operculum, corresponding to the primary gustatory cortex (Rolls, 2015) and overlapping with a local maximum from our mouth/taste localizer. In line with electrophysiology, a recent monkey fMRI study indeed demonstrated taste-related responses in this region (Kaskan et al., 2019).

2.9.5. Seed-based functional connectivity analysis
The resting-state fMRI data included the following additional steps before analysis: (1) bandpass filtering between 0.0025 and 0.05 Hz, (2) regression of white matter and ventricle signals, and their first derivatives, (3) regression of three dimensional motion parameters, and their first derivatives (Mantini et al., 2011; Vincent et al., 2007). The mean representative time course was then obtained by averaging the signal across all the voxels within a seed. Whole-brain connectivity maps were created by calculating the correlations between the signals in the seed and each voxel in the rest of the brain. Individual whole-brain connectivity maps were converted to z scores by Fisher's r-to-z transformation. A fixed-effect analysis was used to create group-level correlation maps (Mantini et al., 2011; Touroutoglou et al., 2016) for the seeds in/near ventral premotor cortex – ventral F5c, dorsal F5c, F5p, F5a, 44 and 44/GrFO. In addition, to test the degree to which resting-state functional connectivity analyses allow retrieval of the hand- and mouth-related functional networks, we also performed a seed-to-brain analyses in motor, parietal, insular and somatosensory regions related to hand and mouth movements. These included medial and lateral F1, area PFG and PF in inferior parietal lobule, posterior and anterior insula,

and lateral and medial portions of S2. The group z score maps were thresholded at z > 2.3 (Hutchison et al., 2015, 2012) and were projected on flattened representations of M12 anatomical template using Caret software (version 5.65).

2.9.6. Correlation matrices

Cross correlation matrices between all seeds were calculated run by run, converted to z scores by Fisher's r-to-z transformation, averaged across runs per monkeys and then across monkeys (Balan et al., 2017; Mantini et al., 2011).

2.9.7. Multidimensional scaling

To visualize the clustering of seed regions, each average z score correlation matrix per monkey was back-transformed to an r matrix by Fisher's z-to -r transformation. This r matrix was rescaled to have values ranging from 0 to 1, and subsequently converted to a distance matrix using 1-r. Nonmetric multidimensional scaling (MDS) using the function mdscale in MATLAB (with the number of dimensions set to 2) was applied to these distance matrices per monkey to visualize them in a 2-dimensional space (Fig. 6A–H).

2.9.8. Circular connectivity graphs

The z scores obtained from the pairwise correlation matrix for F5 and area 44 seeds were used to plot circular graphs to illustrate correlations of the premotor seeds with all other seeds using Matlab's CircularGraph toolbox (Fig. 5C–H).

2.10. GLM analysis for the task-related localizers

A general linear model (GLM) was used to compute the response amplitude at each voxel (Friston et al., 1994; Vanduffel et al., 2001) using SPM5. In order to do this, a MION hemodynamic response function was convolved with a boxcar model representing the various stimulus conditions (Vanduffel et al., 2001). Six motion regressors (three rotations and three translations) along with horizontal and vertical components of the eye movements were included in the GLM as regressors of no-interest to remove motion and eye movement related confounds. A GLM was fitted per run for each voxel resulting in a β map for each condition of interest and for the eight regressors of no-interest. Group analyses (fixed effects) were performed with the level of significance set at $p < 0.05$ corrected (familywise error) for multiple comparisons or at $p < 0.001$, uncorrected. For display purposes, we present SPM T-maps on flattened representations of M12 anatomical template using Caret software (v5.65).

### 2.11. Univariate ROI-based analysis

In the same 2 mm seeds that were used in the resting-state fMRI analysis, we also investigated the functional MR responses during active hand- or mouth movements. Percentage signal changes (an average of all the voxels in these 2 mm seeds) for different contrasts from the hand- and mouth motor localizers (grasp vs. reach execution in the hand movement localizer and sweet liquid vs. artificial saliva in the mouth movement localizer) were calculated using MarsBaR (MarsBaR region-of-interest toolbox for SPM, v0.41).

3. Results

3.1. Functional connectivity of premotor F5 and adjacent area 44 seeds

In order to examine possible variations in functional connectivity of different subparts of F5 with the rest of the brain, we first compared functional connectivity along a dorsal to ventral direction by placing seeds in F5p, dorsal F5c and ventral F5c (red dots in respectively Fig. 2A, B and C). Seeding F5p yielded functional correlations with dorsal F5c and F5a, portions of dorsal premotor regions F2, F3, F6 and F7, premotor F4, hand representations of primary motor F1 and somatosensory S1 cortex, parietal areas PEip, AIP, PF and PFG, and a posterior sector of S2 (Fig. 2A). Anterior to F5p, functional correlations were observed in prefrontal cortex including portions 45 and 46, FEF and cingulate cortices. In contrast, seeding ventral F5c showed functional correlations with lateral/ventral F1 and S1, ventral F4, parietal area PF, medial premotor F5c and F5a, portions of prefrontal and orbitofrontal cortex, portions of S2 and PV, frontal opercular areas DO, PrCO and GrFO, middle and anterior insula, and primary gustatory area (Fig. 2C). Seeding dorsal F5c (Fig. 2B) revealed functional correlations with both hand- and mouth-related areas. These three F5 seeds also yielded functional correlations with distinct visual/superior temporal sulcus regions (Fig. 2A,B,C).

In order to investigate the possibility of systematic variations in the functional resting-state connectivity of F5a and the adjacent fundus, we placed 3 additional seeds in a posterior-to-anterior direction, one seed in the middle of the posterior bank of the arcuate (F5a, Fig. 3A), another seed in to the middle portion of the fundus of the inferior arcuate (area 44, Fig. 3B) and a third seed in the anterior portion of the fundus (44/GrFO, Fig. 3C). The F5a seed revealed functional correlations with neighboring areas F5p, F5c and area 44, and with prefrontal and anterior cingulate regions. Furthermore, functional correlations were observed with portions of GrFO, PrCO, DO and postero-dorsal insula, in addition to F4, S1, S2, parietal areas PF, PFG and AIP, and early visual and posterior STS cortices (Fig. 3A). Area 44, on the other hand, showed functional
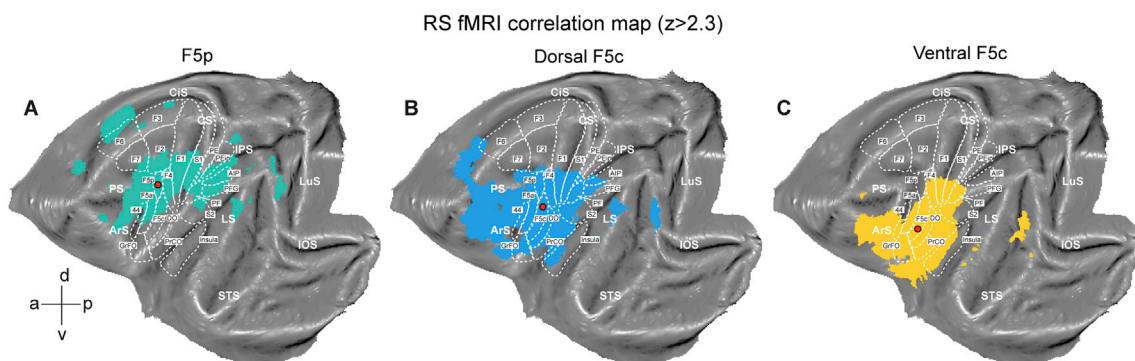
Fig. 2. Resting-state fMRI correlations of ventral premotor F5p, dorsal F5c and ventral F5c. **A.** Left hemisphere resting-state correlation map of a seed placed in F5p. **B.** Left hemisphere correlation map of a seed in the dorsal portion of F5c. **C.** Left hemisphere correlation map of a seed in ventral F5c. Locations of the seeds are denoted by red circles. All maps are thresholded at z > 2.3. White stippled lines indicate locations of various anatomical areas drawn onto the M12 template based on anatomical landmarks and previous functional and anatomical studies (see methods). LuS, lunate sulcus; IOS, inferior occipital sulcus; STS, superior temporal sulcus; IPS, intraparietal sulcus; CS, central sulcus; LS, lateral sulcus; AS, arcuate sulcus; PS, principal sulcus; CiS, cingulate sulcus.
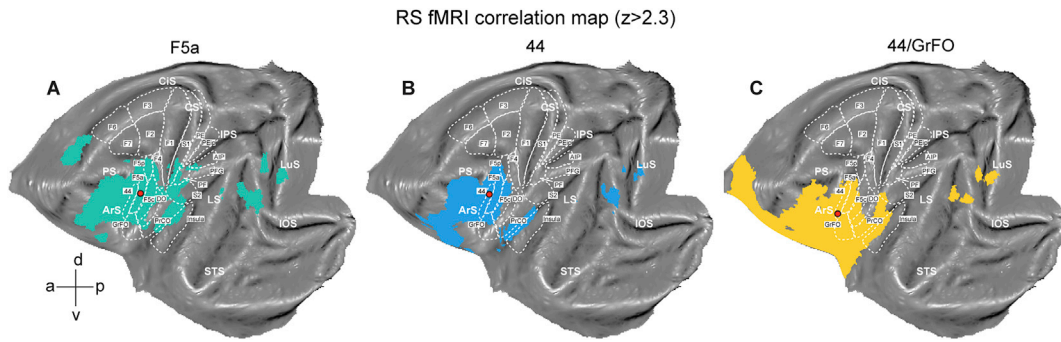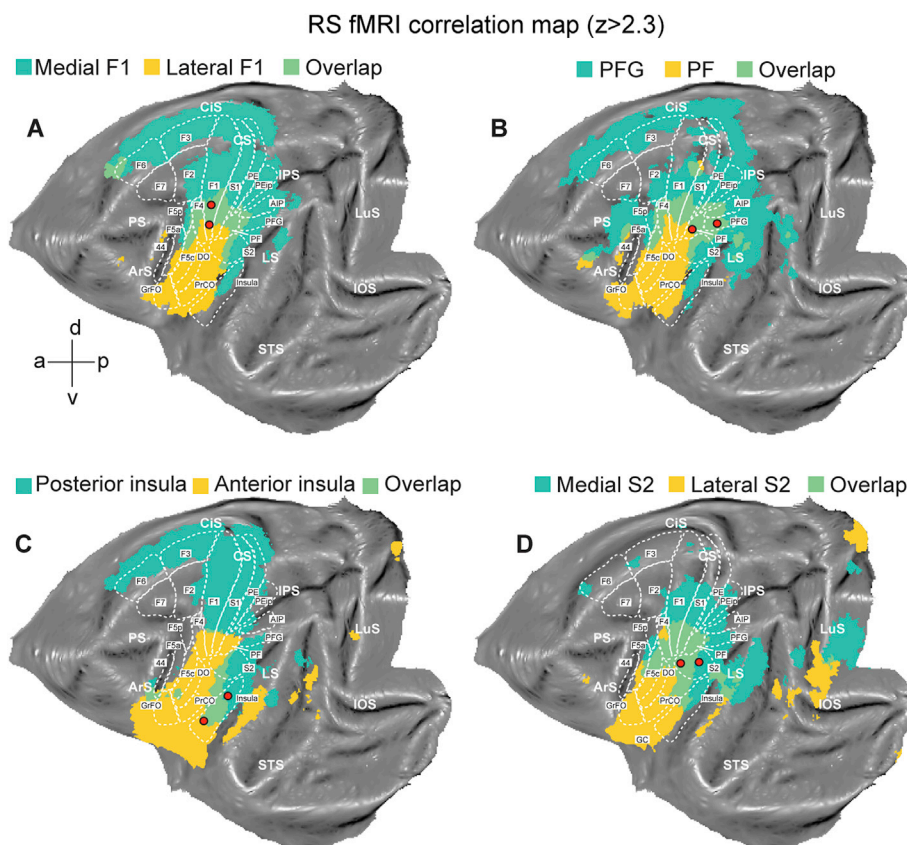
Fig. 3. Resting-state fMRI correlations of F5a, area 44 and 44/GrFO. **A.** Left hemisphere correlation map of a seed placed in F5a. **B.** Left hemisphere correlation map of a seed placed in the middle of the fundus of the arcuate sulcus (area 44). **C.** Left hemisphere correlation map of a seed placed in the anterior tip of the fundus of the arcuate sulcus (44/GrFO). Locations of the seeds are denoted by red circles. All maps are thresholded at z > 2.3. White stippled lines indicate locations of various anatomical areas drawn onto the M12 template based on anatomical landmarks and previous functional and anatomical studies (see methods). LuS, lunate sulcus; IOS, inferior occipital sulcus; STS, superior temporal sulcus; IPS, intraparietal sulcus; CS, central sulcus; LS, lateral sulcus; AS, arcuate sulcus; PS, principal sulcus; CiS, cingulate sulcus.

correlations with F5a and F5c, in addition to prefrontal and orbitofrontal regions, portions of GrFO, PrCO and dorsal insula (Fig. 3B). Contrary to F5a, no significant correlations were observed for this area 44 seed with parietal cortices. Similar to F5a, functional correlations were also observed between the area 44 seed and portions of early visual and posterior STS cortices (Fig. 3B). Finally, the 44/GrFO seed in the anterior fundus showed functional correlations with F5a and ventral F5c, GrFO, portions of DO, PrCO and dorsal insula, in addition to prefrontal and orbitofrontal cortices (Fig. 3C). Similar to the area 44 seed in the middle of the fundus, this anterior 44/GrFO seed also did not yield functional correlations with parietal cortex. As for the F5a and area 44 seed, the 44/GrFO seed showed functional correlations also with portions of early visual and STS cortices. Comparing the seed-to-whole-brain functional correlations of the F5a seed with in particular the anterior 44/GrFO seed

showed a clear shift of functional connectivity with more dorsal regions for the F5a seed (Fig. 3A), to functional connectivity with more ventral regions for the 44/GrFO seed (Fig. 3C).

3.2. Functional connectivity of additional hand- or mouth-related fields

To investigate whether seed-based resting-state functional connectivity analyses is capable of demonstrating functional network specificity of nearby hand- or mouth motor seeds, we performed pair-wise comparisons of resting-state functional connectivity of 1) the hand and mouth representation in primary motor cortex F1/M1 (Fig. 4A) and 2) inferior parietal lobule areas PF and PFG (Fig. 4B) and 3) the dorso-posterior and dorso-anterior insula (Fig. 4C) and 4) the hand and mouth/face sectors of S2 (Fig. 4D). Seeding hand vs mouth-related fields of F1/M1 yielded

Fig. 4. Resting-state fMRI correlations of hand and mouth regions of primary motor cortex F1, parietal areas PF and PFG, posterior and anterior sections of the dorsal insula and lateral and medial portions of S2. **A.** Left hemisphere correlation maps of seeds placed in the hand and the mouth representation of F1 are depicted in turquoise and orange colors, respectively. Regions showing functional correlations with both seeds are shown in green. All maps are thresholded at z > 2.3. White stippled lines indicate locations of various anatomical areas drawn onto the M12 template based on anatomical landmarks and previous functional and anatomical studies (see methods). LuS, lunate sulcus; IOS, inferior occipital sulcus; STS, superior temporal sulcus; IPS, intraparietal sulcus; CS, central sulcus; LS, lateral sulcus; AS, arcuate sulcus; PS, principal sulcus; CiS, cingulate sulcus. **B.** Left hemisphere correlation map of seeds placed respectively in parietal areas PFG and PF. Other conventions same as in A. **C.** Left hemisphere correlation map of seeds placed respectively in dorso-posterior insula and dorso-anterior insula. Other conventions same as in A. **D.** Left hemisphere correlation map of seeds placed respectively in lateral and medial portions of S2. Other conventions same as in A.

largely distinct networks (Fig. 4A), with a portion of F5p, F5a, dorsal F5c, dorsal F4, dorsal premotor cortices F2, F3 and F6, parietal areas AIP, PFG, PE and PEip, medial S1, hand field of S2/PV, dorsal portion of posterior insula, and cingulate cortex, all yielding strong functional correlations with hand motor field of F1 (Fig. 4A). On the other hand, the ventral face/mouth field of F1 showed strong correlations with ventral F5c, a portion of F5a, ventral F4, frontal opercular regions DO, PrCO and GrFO, dorso-anterior insula and the adjacent portion of primary gustatory cortex, ventral S1, parietal PF and the mouth-field of S2/PV (Fig. 4A). Distinct functional correlation maps were also obtained after seeding parietal areas PF and PFG (Fig. 4B). PF in particular showed function correlations with ventral F5c and portion of F5a, frontal opercular regions DO, PrCO, GrFO, dorso-anterior insula, ventral sectors of F1, S1 and F4, and the mouth-field of S2/PV (Fig. 4B). In contrast, PFG showed distinct functional correlations with portions of F5p and F5a, medial F1, portions of dorsal premotor F2, F3 and F6, cingulate cortex, parietal areas AIP, PE, PEip, medial S1, hand field of S2/PV and dorso-posterior insula, in addition to more posterior portions of STS and parietal cortex (Fig. 4B). Comparing resting-state functional connectivity of the anterior with the posterior sectors of the dorsal insula also yielded highly distinct functional connectivity maps (Fig. 4C). The dorso-posterior sector of the insula, where hand grasping-related neurons were recorded (Ishida et al., 2013), yielded distinct functional correlations with hand field of S2/PV, parietal areas PFG, AIP, PE, PEip, medial S1 and F1, in addition to portions of dorsal premotor F2, F3 and F6 and adjacent cingulate cortex. The anterior portion of the dorsal insula, where mouth movements could be elicited using microstimulation (Jezzini et al., 2012), revealed distinct functional connectivity with ventral F1, ventral F4, ventral F5c, opercular regions DO, PrCO and GrFO, gustatory cortex and adjacent orbitofrontal cortex, mouth field of S2/PV, ventral S1, parietal PF and portion of superior temporal gyrus (Fig. 4C). Finally, seeding the lateral portion of S2, where the face and mouth is represented, yielded significant functional correlations with ventral portions of S1, F1 and F4, inferior parietal area PF, premotor F5c and F5a, in addition to dorso-anterior insula, GrFO, PrCO, DO and gustatory cortex (Fig. 4D). Portions of early visual and STS cortex also showed functional correlations with this seed. Seeding the hand representation of S2 on the other hand showed functional correlations with medial parts of F1 and S1, as well as portions of parietal areas PE, PEip, AIP and PFG (Fig. 4D). In premotor cortex, functional correlations were observed in portions of F5p, F5a and dorsal F5c, as well as in discrete portions of dorsal premotor areas F3 and F6. Besides functional correlations with dorso-posterior insula, the S2 hand seed also yielded functional connectivity with posterior upper bank of STS and early visual cortex (Fig. 4D).

3.3. Functional connectivity of premotor F5 and adjacent area 44 seeds with hand- and mouth-somato-motor networks

In addition to investigating seed-brain correlations, we examined resting-state functional correlations between the F5 (and adjacent area 44) seeds (black circles in Fig. 5A) and additional seeds in regions previously shown to be functionally related to either hand or mouth (face) motor movements (Fig. 5A). The seed locations were based upon anatomical landmarks and on previous anatomical and functional studies (see methods). Hand-related seeds included the hand representation of F1, the dorsal sector of F4, hand representations of somatosensory S1 and S2, parietal areas PFG, AIP, PEip and PE, and the posterior portion of the dorsal insula (Fig. 5A, turquoise circles). Mouth-related seeds included the mouth (face) representation of F1, ventral F4, mouth (face) representations in S1 and S2, parietal area PF, frontal opercular regions DO, PrCO and GrFO, the anterior portion of dorsal insula and primary gustatory cortex (Fig. 5A, orange circles). We first computed pairwise correlations between each of these hand and mouth seeds, which were transformed to z-scores and averaged across monkeys. The average z-score correlation matrix is shown as a heat map (Fig. 5B) where red colors indicate highest correlations and dark blue colors indicate lowest

correlations. This correlation matrix shows two clear clusters, indicating high correlations for most of the mouth-related seeds with other mouth-related seeds, and high correlations for hand-related seeds with other hand-related seeds. Examining functional correlations of the F5 (and area 44) seeds with these additional hand and mouth motor seeds showed clearly distinct resting-state functional connectivity profiles (Fig. 5C–H). The ventral portion of F5c yielded strong functional correlations with all mouth motor seeds (Fig. 5C), while F5p showed overall strongest correlations with most of the hand-related seeds (Fig. 5E). Ventral F5c also yielded strong functional correlations with most other F5 seeds, except with F5p. Dorsal F5c displayed strong functional correlations with both the hand- and mouth motor seeds, and with all other F5 and area 44 seeds (Fig. 5D). Similar to F5p, the F5a seed also showed strong functional correlations with several hand-related seeds, including parietal AIP and PFG, dorsal F4 and hand field of S2. In addition, F5a seed yielded functional correlations with mouth field of S1, S2 and F1 (Fig. 5F). The F5a and F5p seeds showed different functional connectivity particularly for posterior insula, parietal areas PE and PEip, hand fields of S1 and F1, area PF and mouth fields of F4 and S2. In addition, while the F5a seed showed strong functional correlations with all other F5 seeds and the area 44 seeds, the F5p seed only yielded weak correlations with ventral F5c and 44/GrFO seeds (Fig. 5E and F). Finally, comparing functional correlations of F5a seed in the posterior bank of the inferior arcuate sulcus with nearby area 44 seed located in the middle of the fundus, showed that both seeds displayed marked differences in their functional connectivity profile. While F5a yielded strong correlations with several hand-related seeds (Fig. 5F), this was not observed for the area 44 (Fig. 5G) or 44/GrFO (Fig. 5H) seeds. Contrary to F5a, in particular the anterior 44/GrFO seed showed strong correlations with several mouth-related seeds, including PrCO, GrCO, anterior insula and gustatory cortex (Fig. 5H).

3.4. Multidimensional scaling

Using multidimensional scaling, we visualized the clustering of the premotor F5 seeds with respect to the additional hand and mouth-related seeds in each of the eight individuals in a 2-dimensional space (Fig. 6A–H). In line with the group correlation matrix (Fig. 5B), in most of the monkey subjects, the hand (turquoise) and mouth-related (orange) seeds grouped together in two distinct clusters. In most individual subjects, the F5p seed clustered with the hand-related seeds and the ventral F5c seed clustered with the mouth-related seeds. In contrast, dorsal F5c and F5a are mostly represented between the hand and mouth-related clusters.

3.5. Task-related functional MRI responses during active hand or mouth movements

Furthermore, in order to compare resting-state functional networks with task-defined functional motor networks, we trained two of the eight monkeys to perform active hand grasping or ingestive mouth movements in the scanner (Fig. 7). During the hand-grasping task, monkey were required to grasp different objects in the dark (Fig. 1A). In the mouth movement localizer, subjects performed mouth movements including licking and jaw movements while receiving a sweet liquid (Fig. 1B). Fig. 7 shows the results (fixed-effects group data) of the hand and mouth movement fMRI localizers. Consistent with previous monkey fMRI grasping studies (Fiave et al., 2018; Nelissen et al., 2018; Nelissen and Vanduffel, 2011; Sharma et al., 2018), contrasting reach-and-grasp with reach-only execution in the dark yielded significant (p < 0.05, FWE corr.) contralateral fMRI responses in ventral premotor cortex including portions of F4, F5p, dorsal F5c, and F5a (Fig. 7A). Grasp-related fMRI responses extended more anteriorly towards the anterior bank of the arcuate sulcus and adjacent convexity (area 45). In addition, significant responses were observed in the hand representation of primary motor cortex (F1) and primary somatosensory cortex S1 (including portions of 3a, 3b, area 1 and 2), extending posteriorly into area 5 (PE and PEip), and
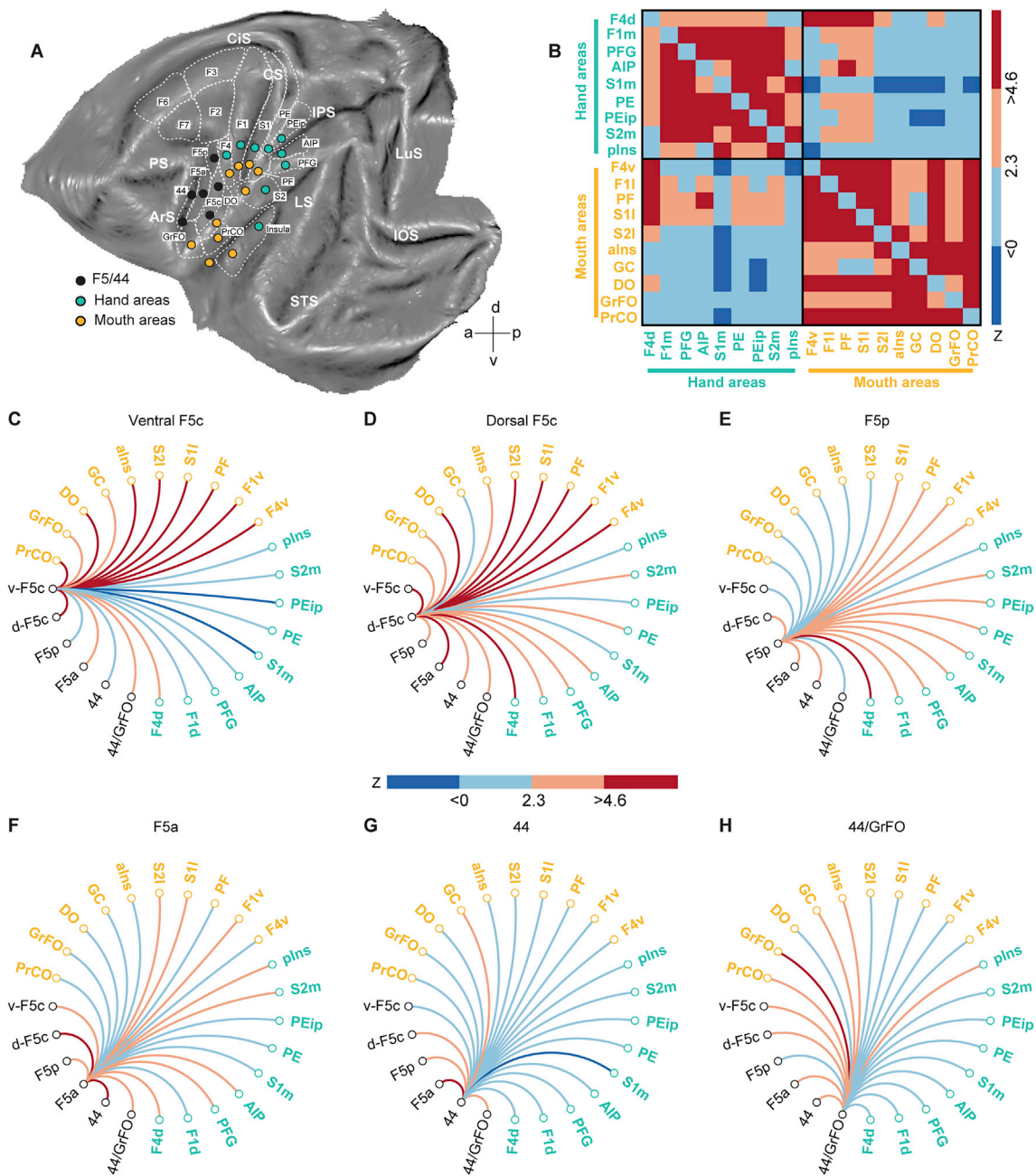
Fig. 5. Resting-state fMRI correlations of F5 subfields with hand and mouth motor networks. **A.** Location of the different seeds investigated in this study, overlaid onto a left hemisphere template flatmap. The turquoise and orange circles indicate locations of seeds in brain regions related to hand and mouth movement, respectively. Black circles represent locations of the premotor F5 and area 44 seeds. **B.** Pairwise z-score correlation matrix between the nine hand and ten mouth motor seeds, shown in A. Blue colors indicate values lower than z = 2.3 and red colors indicate values higher than z = 2.3 (which corresponds to the threshold used for the whole brain correlation maps). **C-H.** Circular connectivity plots displaying functional correlations of F5 and area 44 seeds with hand and mouth motor seeds. Colors of the lines indicate correlation strengths.

in parietal areas AIP and PFG. In the lateral sulcus, responses were found in the secondary somatosensory region S2 (and possibly PV) on the upper bank of the lateral sulcus as well as in posterior insula (Fig. 7A). Comparing ingesting a sweet liquid versus artificial saliva (Fig. 7B) yielded differential fMRI responses in ventral portions of premotor F4 and F5c, in the face representation of ventral F1 and S1, a portion of parietal area PF and in the face representation of S2 on the crown of the upper bank of lateral sulcus. In addition, responses were observed in portions of frontal opercular areas DO, PrCO and GrFO. Finally, significant responses were found in orbitofrontal cortex and the anterior insular regions and adjacent operculum, where the primary taste cortex has been described. In Fig. S1 (Supplementary materials), the location of our F5

and additional hand and mouth motor seeds are shown on top of the hand grasping and mouth movement localizer data. Our hand grasping and mouth movement task localizers confirmed that most seeds were indeed located in/near either hand or mouth movement responsive regions (Supplementary materials, Fig. S1).

3.6. Comparison of task-related fMRI responses and resting-state functional connectivity

To examine the functional specializations of the different F5 premotor seeds with respect to hand or mouth motor movements, we compared resting-state functional correlations and task-related fMRI responses in
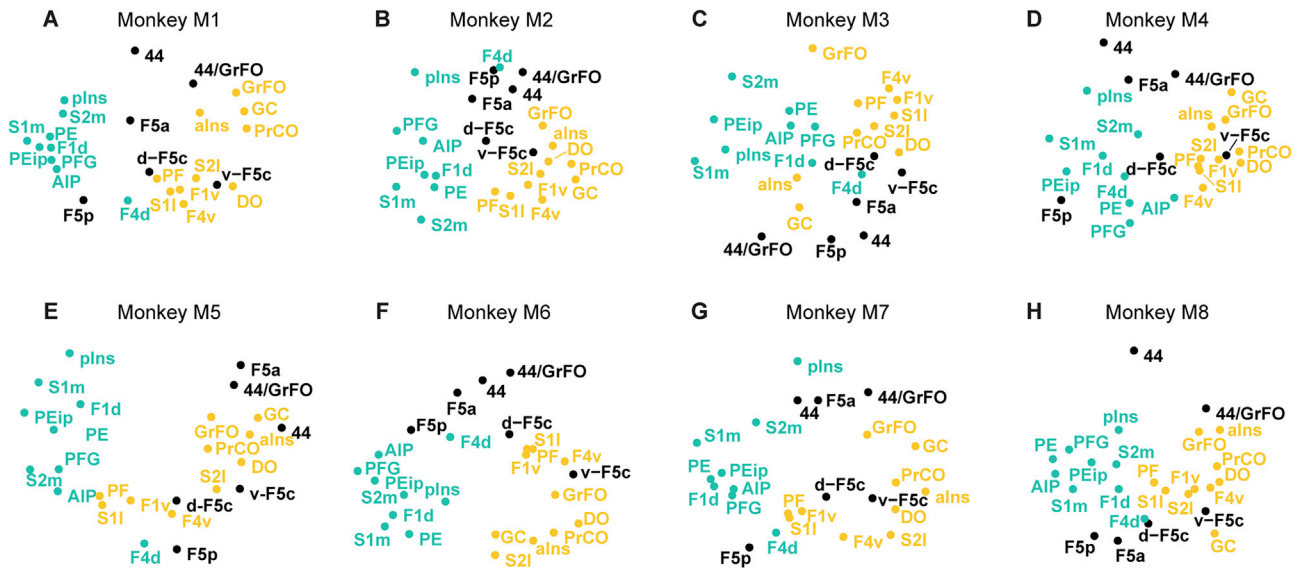
Fig. 6. A-H. Correlation matrices per monkey visualized in a 2-dimensional space using multidimensional scaling. Black: premotor F5 and area 44 seeds. Turquoise: hand motor seeds. Orange: mouth motor seeds.
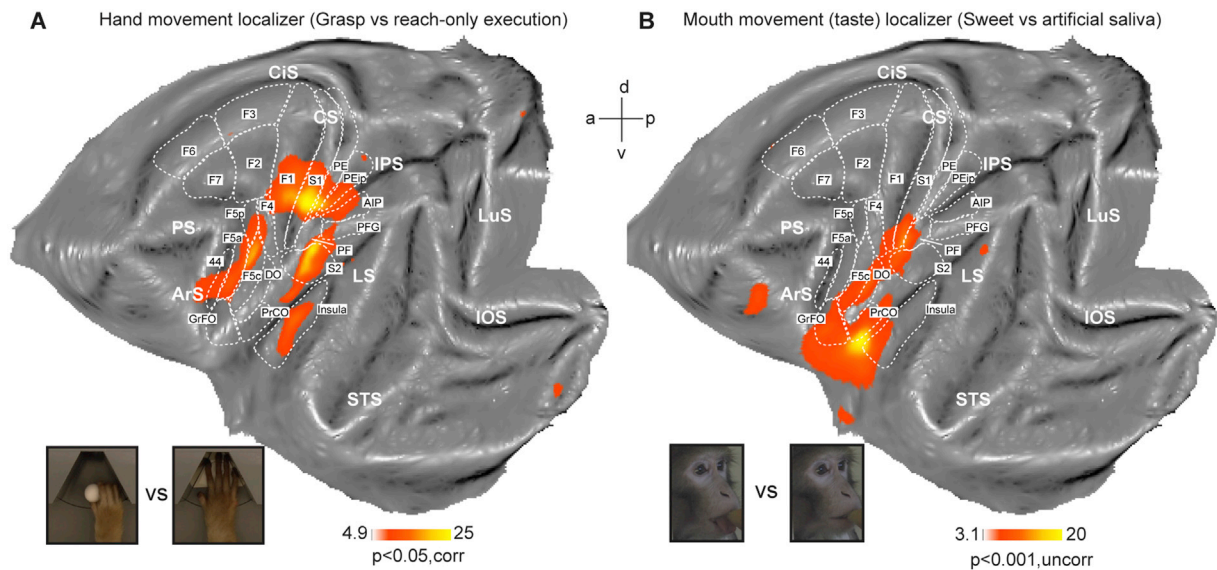
Fig. 7. Hand and mouth movement task-related fMRI localizers. **A, B.** Group data of two monkeys presented on left hemisphere flat maps, showing hand grasping-related (compared to reach-only) fMRI responses (A; p < 0.05, FWE corrected) and mouth movement/taste (compared to artificial saliva) related fMRI responses (B; p < 0.001, uncorrected). White stippled lines indicate locations of various anatomical areas drawn onto the M12 template based on anatomical landmarks and previous functional and anatomical studies (see methods). LuS, lunate sulcus; IOS, inferior occipital sulcus; STS, superior temporal sulcus; IPS, intraparietal sulcus; CS, central sulcus; LS, lateral sulcus; AS, arcuate sulcus; PS, principal sulcus; CiS, cingulate sulcus.
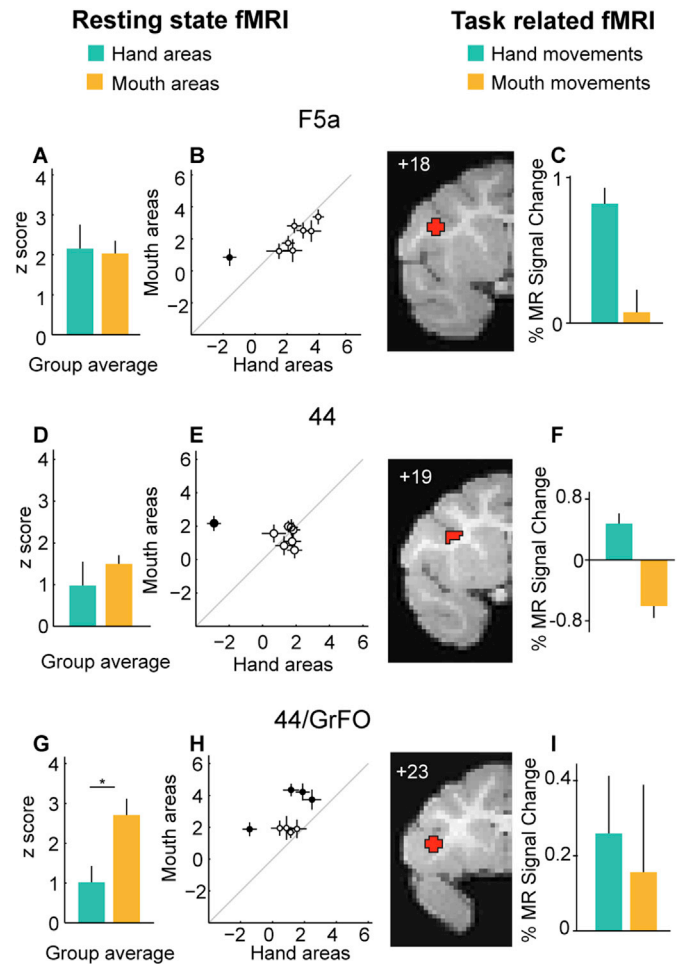
the same seeds (Figs. 8 and 9). Location of the F5 and 44 seeds is shown in red on coronal sections of the MR template (Figs. 8 and 9). For each of the F5 or area 44 seeds, we calculated the average correlation of that seed with all the other hand (nine in total) or mouth-related (ten in total) seed regions (excluding the other F5 and area 44 seeds). This resulted in two values per F5 seed – expressing the average correlations of this seed with, respectively, the nine hand areas or with the ten mouth areas. The ventral portion of premotor F5c yielded significantly stronger correlations with mouth areas compared to hand areas (Fig.8A; t = −7.34; p = 0.00016) while the reverse was true for F5p (Fig.8G; t = 2.69; p = 0.031). On average, dorsal F5c showed significantly stronger correlations with the mouth areas than with the hand areas (Fig.8D; t = −5.12; p = 0.0014). Scatterplots (Fig. 8B, E, and H) show the same correlation results for each of these F5 seeds per individual monkey, where the x-axis represents the

correlation of the F5 seed with hand-related areas and the y-axis represents the correlation with mouth-related areas. Filled circles indicate monkeys displaying a significantly different t statistic at p < 0.05 across runs (Supplementary materials, Table S1). In general, results across runs within monkeys (Fig. 8B, E, and H) match the results observed for the group average across monkeys (Fig. 8A, D, and G). We also plotted the percentage signal change for reach-and-grasp execution vs. reach-only execution from the hand movement localizer and sweet liquid vs. artificial saliva from the mouth movement localizer in these seeds. The ventral F5c seed did not yield hand grasping-related responses but responded during mouth movements (Fig. 8C). Dorsal F5c (Fig. 8F) and F5p (Fig. 8I) on the other hand showed increased MR responses only during execution of hand grasping movements (vs reach-only) and not during active mouth movements.
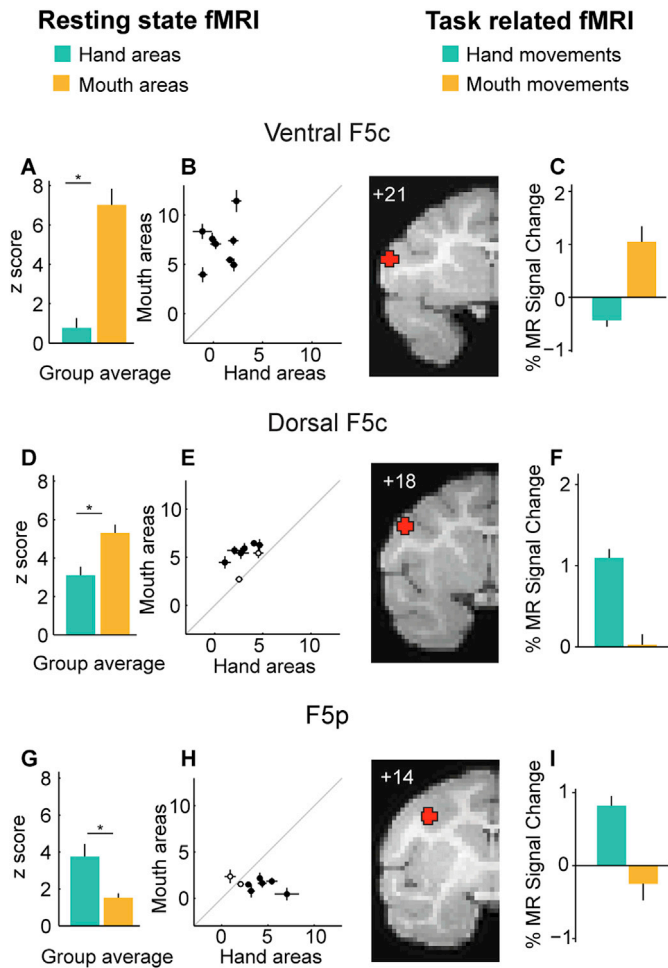
Fig. 8. Comparison of resting-state fMRI correlations and task-related fMRI responses in ventral F5c, dorsal F5c and F5p seeds. **A,D,G**. Correlation of ventral F5c (**A**), dorsal F5c (**D**) and F5p (**G**) seed with the nine hand-related and ten mouth-related seeds. Bar plots show results of the group average of the eight monkeys. Error bars indicate standard error of the mean across monkeys. Asterisks indicate significant differences between the correlations of F5 seed with all other hand versus all other mouth-related areas, at p < 0.05. **B,E,H**. Scatter plots displaying the average correlations for ventral F5c (**B**), dorsal F5c (**E**) and F5p (**H**) seed per monkey across runs. X-axis and Y-axis indicate correlations of F5 seed with hand areas and mouth areas, respectively. Filled circles indicate subjects in which correlations of F5 seed with hand-related areas versus correlation with mouth-related areas is significant (p < 0.05 across runs). Open circles indicate subjects where this difference was not significant (p > 0.05). Crosses on the circles are error bars indicating standard error of the mean across runs. **C,F,I**. Percentage signal change for reach-and-grasp execution vs. reach-only execution (turquoise) and sweet liquid vs artificial saliva (orange) plotted in the ventral F5c (**C**), dorsal F5c (**F**) and F5p (**I**) seeds. Error bars indicate standard error of the mean across runs.

Fig. 9. Comparison of resting-state fMRI correlations and task-related fMRI responses in F5a, area 44 and 44/GrFO. **A, D, G**. Correlation of F5a (**A**), area 44 (**D**) and 44/GrFO (**G**) seeds with the nine hand-related and ten mouth-related seeds. Bar plots show results of the group average of the eight monkeys. Error bars indicate standard error of the mean across monkeys. Asterisks indicate significant differences between correlations of each seed with all other hand versus all other mouth-related areas at p < 0.05. **B, E, H**. Scatter plots displaying the average correlations for F5a (**B**), area 44 (**E**) and 44/GrFO (**H**) seed per monkey across runs. X-axis indicates correlation of seed with hand areas and y-axis indicates correlation of that seed with mouth areas. Filled circles indicate subjects in which correlations of the seed with hand-related areas versus correlation with mouth-related areas is significantly different (p < 0.05 across runs). Open circles indicate subjects where this difference was not significant (p > 0.05). Crosses on the circles are error bars indicating standard error of the mean across runs. **C,F,I**. Percentage signal change for reach-and-grasp execution vs. reach-only execution (turquoise) and sweet liquid vs artificial saliva (orange) plotted in the F5a (**C**), area 44 (**F**) and 44/GrFO (**I**). Error bars indicate standard error of the mean across runs.

Functional correlations of the F5a seed with the hand or mouth-related seeds were not significantly different at the group level (Fig.9A; t = 0.30, p = 0.77) nor in most of the individuals (Fig. 9B). With respect to task-fMRI, premotor F5a yielded strong fMRI responses during hand grasping (vs reach-only) but not during mouth movements (Fig. 9C). Correlations of the area 44 seed with hand-related or mouth-related seeds was not significantly different at group level (Fig.9D; t = −0.74, p = 0.48) nor in most individual subjects (Fig. 9E, Supplementary materials, Table S2). This seed in the middle of area 44 yielded modest hand grasping-related responses (Fig. 9F). Finally, the 44/GrFO seed in the anterior tip of the fundus of the arcuate yielded significantly stronger correlations with mouth-related regions compared to hand-related regions, at the group level (Fig.9G; t = −4.24, p = 0.0039) and in 4 of the

individual subjects (Fig. 9H, Table S2). In addition, only modest MR responses were observed during both our functional hand and mouth movement tasks in this seed (Fig. 9I).

We performed a similar comparison of resting-state functional connectivity and task-related fMRI responses in the pairs of F1, parietal, insular and S2 seeds, for which seed-to-brain correlation maps were shown in Fig. 4. For the resting-state correlation analysis, we compared correlations of these seeds (medial F1 and lateral F1, PFG and PF, dorso-posterior insula and dorso-anterior insula, lateral and medial S2) by averaging z scores across the remaining eight hand-related and remaining nine mouth-related (excluding the premotor/44 seeds). Resting-state functional correlation analysis confirmed a stronger correlation between the medial F1 seed and other hand-related regions (compared to mouth-

related regions), with the opposite being observed in lateral/ventral F1 (Fig. 10A; medial F1: t = 3.54, p = 0.0094; lateral/ventral F1: t = −5.90, p = 0.0006). This dissociation was also observed in most of the individual subjects (Fig. 10B and C; Supplementary materials, Table S3). In line with its known topography and functional specialization, the seed in the medial portion of F1 showed robust responses during hand grasping, whereas mouth movements did not elicit any fMRI responses in this seed

(Fig. 10D). The reverse was true for the lateral portion of F1, where the face and mouth are represented. As expected, this seed showed mouth movement related fMRI responses and failed to respond while monkeys performed hand-grasping actions (Fig. 10D).

Comparable to the two seeds in primary motor F1, a similar task and resting-state defined functional specialization could be observed for the two inferior parietal lobule regions PF and PFG. Area PFG yielded
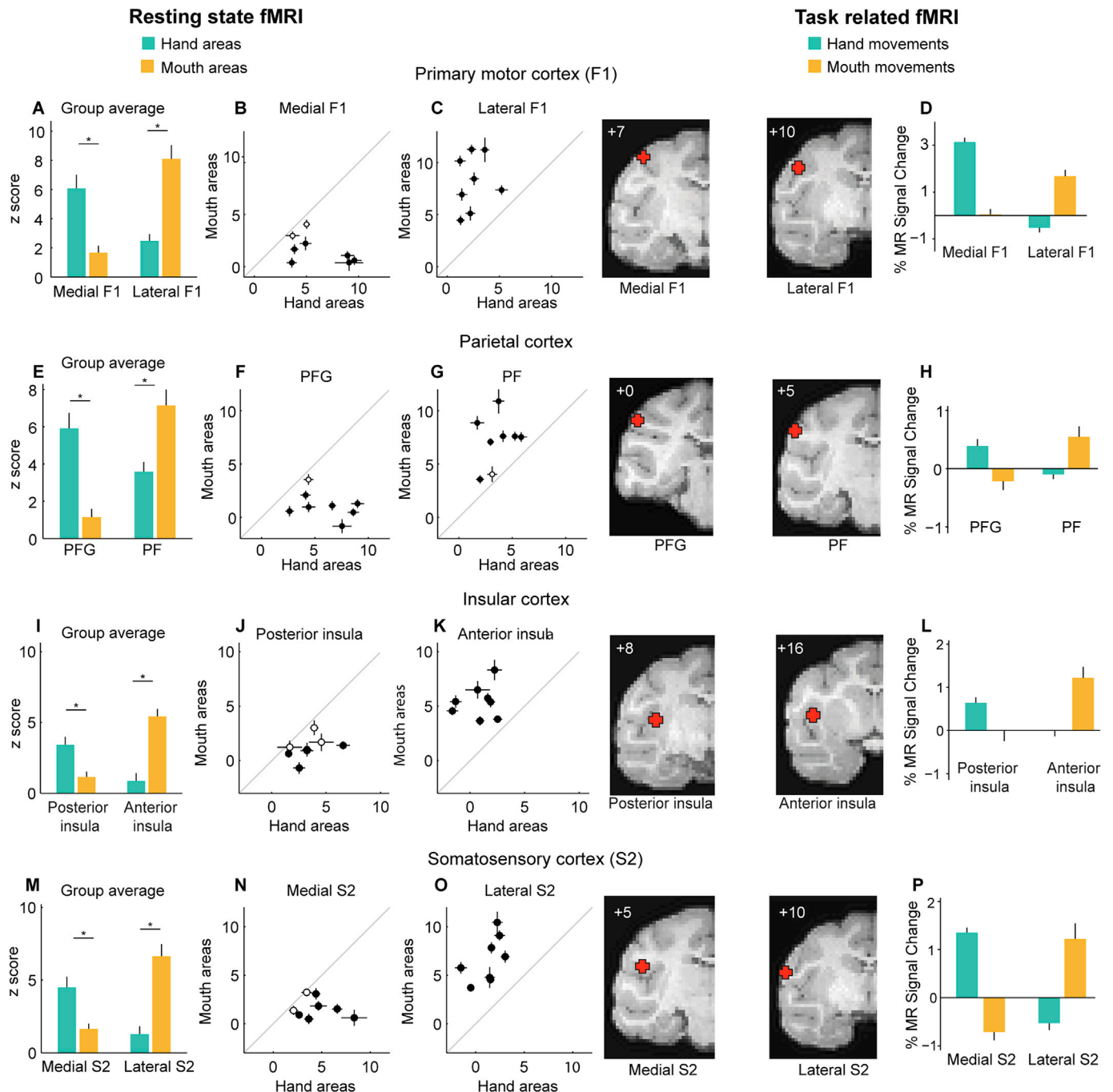
Fig. 10. Comparison of resting-state fMRI correlations and task-related fMRI responses in primary motor, inferior parietal lobule, insular and S2 seeds. **A, E, I, M**. Correlation of motor (**A**), parietal (**E**), insular (**I**) and somatosensory S2 (**M**) seeds with other hand- and mouth-related seeds. Bar plots show results of the group average of the eight monkeys. Error bars indicate standard error of the mean across monkeys. An asterisk indicates a significant difference between correlation of each seed with all other hand versus all other mouth-related areas at p < 0.05. **B, C, F, G, J, K, N, O**. Scatter plots displaying the average correlations per monkey across runs. X-axis indicates correlation of that seed with hand areas and y-axis indicates correlation of the same seed with mouth areas. Filled circles indicate subjects in which correlation of the seed with hand-related areas versus correlation with mouth-related areas is significant (p < 0.05 across runs). Open circles indicate subjects where this difference was not significant (p > 0.05). Crosses on the circles are error bars indicating standard error of the mean across runs. **D, H, L, P**. Percentage signal change for reach-and-grasp execution vs. reach-only (turquoise) and sweet liquid vs artificial saliva (orange) plotted in medial and lateral F1 (**D**), parietal areas PFG and PF (**H**), posterior and anterior insula (**L**) and medial and lateral S2 (**P**). Error bars indicate standard error of the mean across runs.

responses exclusively during hand grasping (Fig. 10H) and showed significantly stronger correlations with other hand (compared to mouth) regions (Fig.10E; t = 4.41, p = 0.0031). Area PF on the other hand was particularly responsive during mouth movements (Fig. 10H) and the PF seed correlated more strongly with mouth-related than with hand-related seeds during resting-state fMRI (Fig.10E; t = −4.10, p = 0.0045). This dissociation between the strengths of the correlations with hand and mouth motor networks was observed in most individuals (Fig. 10F and G; Supplementary materials, Table S4). Hand grasping elicited fMRI responses in dorso-posterior, but not dorso-anterior insula, while the opposite was true for the mouth movements (Fig.10L). This functional specialization was also evident from investigating resting-state correlations showing, at the group level, significantly stronger correlations between the dorso-anterior insula and mouth-related regions (compared to hand-related regions; t = −6.60, p = 0.0003), and the reverse for the dorso-posterior insula seed (Fig.10I; t = 4.13, p = 0.0044). At the individual level, the difference in correlation strengths between the two motor networks was especially apparent for the dorso-anterior insula seed (Fig. 10K), with all individual subjects showing this same result. For the posterior insula seed, this dissimilarity in correlation strengths with hand- and mouth motor networks was significant only in five out of eight subjects (Fig. 10J, Supplementary materials, Table S5). Finally, similar to F1, anterior parietal and insula seeds, a distinct functional specialization was also evident for the S2 hand and mouth seeds. At group level, the medial S2 seed yielded significantly stronger functional correlations with the hand-related regions (compared to mouth-related regions), while the reverse was observed for the lateral S2 seed (Fig.10M; medial S2, t = 3.24, p = 0.014; lateral S2, t = −7.64, p = 0.00012). At the single subject level, significant differences in functional correlations with hand- or mouth-related networks were observed in 6 out of 8 subjects for the medial (hand) S2 seed (Fig.10N, Supplementary materials, Table S6), and in all subjects for the lateral (mouth) S2 seed (Fig.10O, Table S6). In line with these functional connectivity observations, the medial S2 seed yielded robust MR signal changes during active hand movements, while mouth movements did not elicit above baseline responses (Fig.10P). The opposite pattern of functional responses was observed in the lateral S2 seed (Fig.10P).

4. Discussion

In this study we investigated the functional specialization of macaque premotor F5 subfields with respect to hand and non-communicative mouth movements, using both seed-based resting-state fMRI (Babapoor-Farrokhran et al., 2013; Balan et al., 2017; Hutchison et al., 2011; Mantini et al., 2011; Neubert et al., 2014) and task-related fMRI during which monkeys either grasped objects in the dark with their right hand or performed licking and ingestive movements while receiving a sweet liquid.

4.1. Cytoarchitectonic organization of ventral premotor F5 in the macaque

The architectonic organization of the ventral premotor cortex in the macaque has been studied by several authors over the course of the last century. Some authors have suggested that this part of the cortex consists of distinct areas located at different dorso-ventral levels (Vogt and Vogt, 1919; Barbas and Pandya, 1987; Preuss and Goldman-Rakic, 1991). Others have suggested an organization consisting of several areas located at different rostro-caudal levels (von Bonin and Bailey, 1947; Matelli et al., 1985). According to Matelli et al. (1985), macaque ventral premotor cortex consist of a caudal (F4) and a rostral (F5) sector, largely corresponding to FBA and FCBm sectors of von Bonin and Bailey (1947). Recently, based upon cyto- and chemoarchitectonic techniques (Belmalih et al., 2007), area F5 as defined by Matelli et al. (1985), could be further subdivided into three sectors: F5c (convexity), located on the postarcuate cortex adjacent to the inferior arcuate sulcus, F5p (posterior) in the posterior sector of the posterior bank of the inferior arcuate, and F5a

(anterior) in a more anterior portion of the posterior bank of the inferior arcuate (Belmalih et al., 2009; Nelissen et al., 2005).

4.2. Functional responses in F5 subfields

Area F5 is generally considered a key region of the parieto-frontal lateral grasping circuit (Borra et al., 2017). This circuit is involved in coding visuomotor transformations necessary for grasping, by transforming visual object properties including size, shape and orientation into potential motor acts for appropriate hand-object interactions (Jeannerod et al., 1995; Rizzolatti and Luppino, 2001). It has been shown that F5 contains not only a motor representation of the hand but also of the mouth, both of which seem to overlap to a considerable extent (Ferrari et al., 2017; Gentilucci et al., 1988; Hepp-Reymond et al., 1994; Kurata and Tanji, 1986; Maranesi et al., 2012; Rizzolatti et al., 1988). While neuronal activity in F5p is mostly hand-related, F5c shows a transition from hand-to mouth-related responses from dorsal to ventral regions (for review, see Ferrari et al., 2017). Functional responses in F5a, the most anterior F5 sector in the posterior bank of the arcuate, has been studied less intensively than have F5c and F5p. Monkey fMRI studies have suggested both 3D shape (Joly et al., 2009) and grasping-related (Nelissen and Vanduffel, 2011) responses in this sector. A follow-up electrophysiological study confirmed the presence of both disparity-selective and grasping-related motor responses in F5a (Theys et al., 2012). Many of the 3D shape-selective neurons in F5a were also active during visually guided grasping (as opposed to grasping in the dark), which suggests a specific role for F5a in the visual analysis of 3D object properties related to object grasping (Schaffelhofer and Scherberger, 2016; Theys et al., 2012). In agreement with previous macaque single-cell and neuroimaging data, our hand-grasping localizer yielded significant ventral premotor responses related to grasp execution in the dark, in all three sectors of F5 (Fig. 7A). With respect to F5c, these responses were mostly restricted to the dorsal sector (Fig. 7A). It will be interesting for future fMRI investigations to examine to what respect grasping with the mouth yields fMRI responses in these different macaque F5 subfields.

As mentioned above, in addition to the dorsal hand field, F5c also contains a ventral mouth motor field (for review, see Ferrari et al., 2017). Ferrari et al. (2003) described the presence of motor neurons in F5c, those discharging during execution of mouth actions related to ingestive functions like grasping, sucking or breaking food with the mouth. A small number of neurons in this ventral region also fired during execution of communicative gestures, including lipsmacking. Ventral premotor fMRI responses during face movements and lip smacking have also been demonstrated recently in macaques by Shepherd and Freiwald (2018), although the exact correspondence of their data with respect to the different sectors of F5 or area 44 is not clear. A recent study suggests that some neurons in this portion of F5c, besides responding during mouth related motor responses such as licking, sucking, biting and chewing, also responded during conditioned vocalizations (Coudé et al., 2011). So far, orofacial responses have not been systematically investigated in F5a, although in the neighboring dysgranular area 44 (Petrides and Pandya, 1994), located in the fundus of the inferior arcuate sulcus, and in adjacent prefrontal area 45, orofacial responses related to tongue and jaw movements or neural responses related to vocalizations have been described (Hage and Nieder, 2015; Petrides et al., 2005). Our mouth movement related fMRI data are in agreement with previous single-cell studies in F5. Mouth movements related to licking and ingesting a liquid reward particularly activated the ventral sector of F5c (Fig. 7B). None of the other F5 sectors showed a differential fMRI response during this particular task.

4.3. Functional MR responses in other regions

Overall the results of our fMRI hand grasping localizer are in good agreement with comparable previous motor fMRI experiments in

monkeys (Nelissen and Vanduffel, 2011; Nelissen et al., 2018; Fiave et al., 2018). Contrasting grasping with the right hand in the dark versus reach-only actions, yielded pronounced activations in the so-called lateral grasping network (Borra et al., 2017) in the contralateral hemisphere, including somatosensory, motor, parietal, premotor, and prefrontal cortices (Fig. 7A). The contribution of dorsal premotor and prefrontal regions in planning and execution of hand movements becomes particularly evident when hand movements are contrasted with a fixation baseline (Fiave et al., 2018), instead of *reach-and-grasp* vs. *reach-only* as done here (see also Nelissen and Vanduffel, 2011). In line with previous single cell and microstimulation experiments in macaques (Ishida et al., 2013; Jezzini et al., 2012), the dorso-posterior sector of the insula yielded functional MR responses in particular during active grasping movements with the hand (Fig. 7A). Our mouth movement related fMRI localizer yielded robust differential responses in a number of regions previously indicated as coding mouth movements or taste. Besides mouth/face sectors of F1, F4 and somatosensory cortices, frontal opercular areas such as GrFO, PrCO and DO also showed robust responses, in line with previous studies that have associated these areas with ingestive mouth actions and sensorimotor control of the mouth (Ferrari et al., 2003; Gerbella et al., 2016; Kaskan et al., 2019; Krubitzer et al., 1995; Ogawa, 1994; Ogawa et al., 1989). Functional mouth movement/taste responses were also observed in the most anterior sector of the dorsal insula, in line with observed ingestive behavioral responses following microstimulation in this region by Jezzini et al. (2012).

It should be noted however, that although our mouth motor localizer was able to demonstrate responses in a large number of areas related to coding mouth movements, we compared mouth movements during ingestion of a sweet reward versus mouth movements during ingestion of artificial saliva. This contrast therefore did not exclusively yield mouth movement related responses but also taste-related responses, as clearly evident in the robust fMRI activation in primary gustatory cortex and adjacent insular and orbitofrontal cortex (Fig. 7B; Scott et al., 1986; Rolls et al., 1990; Yaxley et al., 1990; Rolls, 2015; Kaskan et al., 2019). Conceivably, when comparing tasks with versus without mouth movements (Shepherd and Freiwald, 2018), one might expect even larger differential responses in F5 and other regions. Notably, we failed to observe mouth-related responses in medial face regions – M2 or supplementary motor area, and two cingulate areas - M3 and M4, located at different rostral-caudal positions of the midcingulate dorsal to the corpus callosum (Gothard, 2014; Morecraft et al., 2004). This might be because supplementary motor cortex and cingulate area M3 are involved in controlling the upper facial musculature (Morecraft et al., 2004) which was not specifically tested in our task-related fMRI experiment. Moreover, these regions receive strong limbic input and are more related to communicative face movements such as lip smacking and facial expressions compared to non-communicative movements such as drinking and ingestive motions (Nieder, 2018; Shepherd and Freiwald, 2018; Vogt, 2009).

4.4. Functional specializations of macaque F5 based upon resting-state fMRI examinations

Resting-state fMRI investigations, which typically examine temporal correlations of low frequency fluctuations in the BOLD signal in the absence of a specific task paradigm (Biswal et al., 1995), have become a popular tool to investigate the functional organization of the human and non-human primate brain. As opposed to hypothesis-driven, seed-based resting-state analyses (Mantini et al., 2011; Neubert et al., 2014), a few resting-state fMRI studies in the monkey have employed exploratory or data-driven clustering methods such as independent component analysis (ICA) to examine functional connectivity in frontal cortices including premotor F5 (Goulas et al., 2017; Hutchison et al., 2011; Vijayakumar et al., 2018). While both methods are useful (Cole et al., 2010; van den Heuvel and Hulshoff Pol, 2010), so far these data-driven clustering methods (Goulas et al., 2017; Hutchison et al., 2011; Vijayakumar et al.,

2018) have not demonstrated the same level of specialization in F5 as suggested based upon previous mentioned cytoarchitectonic or behavioral single cell or neuroimaging examinations. For instance, using independent component analysis, Hutchison et al. (2011) demonstrated a resting-state network (RSN) cluster including most of the ventral premotor cortex without a clear distinction between hand and mouth-related functional networks (RSN A cluster of Hutchison et al., 2011). More recently, Goulas et al. (2017) also used a data-driven connectivity approach to parcel frontal cortex in the macaque. They found several clusters in lateral frontal cortex, including two functional networks they refer to as (area) 44 and F5c. A cluster for cytoarchitectonic subdivisions F5p and F5a was not described in that study but given that the F5c and area 44 clusters of Goulas et al. (2017) seem to be adjacent, F5a might be partially included in either the area 44 or F5c clusters. Finally, a very recent study also used data-driven clustering methods to examine the organization of the parietal-frontal cortices in the macaque (Vijayakumar et al., 2018). Their clustering algorithm retrieved a dorsal cluster attributed to premotor F4 in addition to a large ventral region attributed to area F5. This F5 cluster seemingly extended towards the lateral convexity of the frontal operculum and, according to recent cytoarchitectonic maps (Gerbella et al., 2016), possibly includes GrFO, PrCO and DO. Anterior to their F5 cluster, the authors described another cluster suggested to correspond to area 44. The tri-partite cytoarchitectonic division of F5 (Belmalih et al., 2009) or the suggested hand vs. mouth-dominated connectivity dichotomy in F5 is not evident from the parcellation scheme suggested by Vijayakumar et al. (2018). While data-driven resting-state parcellations are clearly of interest in understanding the functional specialization of the brain, our and other (Babapoor-Farrokhran et al., 2013; Neubert et al., 2014) studies show that seed-based resting-state fMRI analysis can suggest levels of functional organization that are so far not easily retrieved from data-driven exploratory approaches. It is possible, however, that future investigations increasing the predefined number of clusters in data-driven resting-state approaches might also yield a more fine-grained level of functional specialization in macaque ventral premotor cortex.

4.5. Comparison of F5 resting-state functional connectivity with F5 anatomical tract-tracing data

As mentioned before, resting-state fMRI is based upon correlations of low-frequency fluctuations in the fMRI signals between brain areas (Biswal et al., 1995). Therefore it does not necessarily reflect functionally connected areas that are also monosynaptically linked (Fox and Raichle, 2007; Grandjean et al., 2017). Nonetheless, it has been shown that functional connectivity is, to some extent, constrained by the underlying anatomical architecture (Babapoor-Farrokhran et al., 2013; Damoiseaux and Greicius, 2009; Greicius et al., 2009; Honey et al., 2009; Hutchison et al., 2012, 2011; Margulies et al., 2009; Miranda-Dominguez et al., 2014; Shen et al., 2012; Wang et al., 2013).

As both seed-based functional connectivity measures and tracer tractography depend to a large degree on the location of the seed/injection region, direct comparisons or quantifications of functional connectivity and tracer tractography of macaque F5 is not straightforward (but see Wang et al., 2013). However, our resting-state functional correlation analyses of the different F5 subregions are in good agreement with what is currently known about anatomical connections of macaque F5 (Ferrari et al., 2017; Gerbella et al., 2011). Comparison of resting-state functional correlations specifically with distinct nodes from the hand and mouth motor networks, showed ventral F5c to have the overall strongest correlations with other mouth-related regions, including frontal opercular regions GrFO, PrCO and DO, ventral sectors of F4 and F1, somatosensory areas SI and SII, and inferior parietal area PF (Fig. 5C). This connectivity profile is also evident in tracer studies in the macaque (see Fig. 15 of Gerbella et al., 2011). Indicative of their role in coding hand grasping movements, the dorsal sector of F5c and F5p yielded strong functional correlations with hand-related parietal areas PFG and AIP,

somatosensory regions, dorsal F4 and F1, in line with tracer studies (Borra and Luppino, 2017; Gerbella et al., 2011). Compared to F5c, F5p showed weak functional correlations with frontal opercular regions (Fig. 5C–E). These findings are to a large degree comparable to the connectivity profile of F5p based upon tracer injections (Borra et al., 2008; Gerbella et al., 2011; Ghosh and Gattera, 1995; Kurata, 1991; Matelli et al., 1986). In addition, the suggested connectivity of F5p with dorsal premotor regions F2, F3, F6 and F7 (see Fig. 15 of Gerbella et al., 2011), could be reconstructed with our seed-based correlation assessments of F5p (Fig. 2A). Overall, both our task-related and resting-state data support the proposed shift from a hand movement functional specialization in F5p towards a mouth movement specialization in ventral F5c (Ferrari et al., 2017). Tracer injections in F5a have shown that F5a is connected to hand-related areas AIP, PFG and S2 hand field, in addition to the frontal opercular areas GrFO, PrCO, premotor F4 and F6, insula and ventrolateral prefrontal cortex (Gerbella et al., 2011). Our seed-to-seed correlations of F5a with AIP, PFG and F4, in addition to S2 and insula (Fig. 5F) are in line with these anatomical tractography observations. In line also with tracer injections in F5a, seed-to-brain functional correlations of our F5a seed (Fig. 3A) also showed strong correlations with ventrolateral cortex and portions of GrFO and PrCO.

An intriguing observation that emerged from our seed-to-brain correlation analyses concerns the apparent functional connectivity for all F5 and area 44 seeds with portions of early visual and STS cortices (Figs. 2 and 3). While tracer studies have shown some labeling in portions of STS after F5a or area 44 injections (Frey et al., 2014; Gerbella et al., 2011), future studies will be needed to investigate if these suggested variations in premotor-STS functional resting-state correlations reflect underlying mono- or polysynaptic anatomical connections.

4.6. Comparison of premotor F5a with adjacent area 44

Our data provided additional support for the suggestion that the fundus of the inferior arcuate sulcus in the macaque contains a field that differs from premotor F5a in the posterior bank of the inferior arcuate (Belmalih et al., 2009; Neubert et al., 2014; Petrides et al., 2005). Cytoarchitectonic investigations suggest that the fundus of the inferior arcuate contains a faint layer IV, as opposed to both prefrontal area 45 in the anterior bank of the inferior arcuate that possesses a well-developed layer IV, and area F5a in the posterior inferior arcuate, which typically lacks a layer IV altogether (Petrides and Pandya, 1994; Petrides et al., 2005; Belmalih et al., 2009). This fundal area corresponds to dysgranular area 44 (Petrides and Pandya, 1994) which contains an orofacial representation (Petrides et al., 2005). While our task fMRI data suggest only modestly differential responses during hand and mouth movements in the area 44 seeds (Fig. 9F,I), it is possible that this region might respond more profoundly during communicative face movements including lip smacking (Petrides et al., 2005; Shepherd and Freiwald, 2018) or vocalizations (Hage and Nieder, 2013).

A direct comparison of the anatomical connections of F5a and area 44 in the same monkey subjects has not been performed. Petrides and co-workers (2014) suggest that area 44 has significant connections with F5a (area 6VR) and with anterior parietal cortex including AIP and PFG, in addition to prefrontal 45 and 46v, S2, insula and area ProM (which overlaps with PrCO according to Barbas and Pandya, 1987, see also Gerbella et al., 2016). In addition, modest connections with the fundus of the STS were described (Frey et al., 2014). Injections into the F5a sector on the posterior bank of the inferior arcuate (Gerbella et al., 2011) suggested several shared connections between F5a and area 44, which is reflected also in our current study and other seed-to-brain functional correlation investigations (Neubert et al., 2014). Our functional correlation analysis also suggests that in particular the anterior 44/GrFO seed has strong functional links with other mouth-related regions (Fig. 9G and H) and that there are some fundamental differences in functional connectivity between area 44 and adjacent F5a (see also Neubert et al., 2014). Most particularly, while our F5a seed yielded significant

correlations with premotor F4, somatosensory S2 as well as AIP and PFG in the parietal cortex, this was not observed for our area 44 seeds. Conceivably, the spread of tracers across areal boundaries for injections near the border of area 44 and F5a might have underestimated their unique connectivity profiles.

5. Conclusion

In this study we investigated the functional specialization of macaque F5 subfields with respect to hand and mouth movements, using both seed-based resting-state and task-based fMRI. In line with invasive single cell investigations, task-based fMRI suggests a role for F5p, dorsal F5c and F5a in the execution of hand grasping movements, while in contrast mouth movements elicited responses in the ventral portion of F5c. Resting-state fMRI analyses supports both these task-based functional specializations as well as invasive anatomical tracer data. While F5p showed predominant functional correlations with the hand motor network, ventral F5c showed strong functional correlations with the mouth motor network. Furthermore, our resting-state investigations provide additional evidence for a different functional specialization of premotor F5a and neighboring area 44 in the inferior arcuate sulcus. Overall, our study supports the use of non-invasive resting-state fMRI to examine functional networks in the brain and shows that seed-based resting-state fMRI analysis can suggest levels of functional organization that are not easily retrieved from data-driven exploratory approaches.

Appendix A. Supplementary data

Supplementary data to this article can be found online at https://doi.org/10.1016/j.neuroimage.2019.02.045.

References

Babapoor-Farrokhran, S., Hutchison, R.M., Gati, J.S., Menon, R.S., Everling, S., 2013. Functional connectivity patterns of medial and lateral macaque frontal eye fields reveal distinct visuomotor networks. J. Neurophysiol. 109, 2560–2570. https://doi.org/10.1152/jn.01000.2012.

Balan, P.F., Gerits, A., Mantini, D., Vanduffel, W., 2017. Selective TMS-induced modulation of functional connectivity correlates with changes in behavior. Neuroimage 149, 361–378. https://doi.org/10.1016/j.neuroimage.2017.01.076.

Barbas, H., Pandya, D.N., 1987. Architecture and frontal cortical connections of the premotor cortex (area 6) in the rhesus monkey. J. Comp. Neurol. 256, 211–228. https://doi.org/10.1002/cne.902560203.

Belmalih, A., Borra, E., Contini, M., Gerbella, M., Rozzi, S., Luppino, G., 2007. A multiarchitectonic approach for the definition of functionally distinct areas and domains in the monkey frontal lobe. J. Anat. 211, 199–211. https://doi.org/10.1111/j.1469-7580.2007.00775.x.

Belmalih, A., Borra, E., Contini, M., Gerbella, M., Rozzi, S., Luppino, G., 2009. Multimodal architectonic subdivision of the rostral part (area F5) of the macaque ventral premotor cortex. J. Comp. Neurol. 512, 183–217. https://doi.org/10.1002/cne.21892.

Biswal, B., Zerrin Yetkin, F., Haughton, V.M., Hyde, J.S., 1995. Functional connectivity in the motor cortex of resting human brain using echo-planar mri. Magn. Reson. Med. 34, 537–541. https://doi.org/10.1002/mrm.1910340409.

Bonini, L., Maranesi, M., Livi, A., Fogassi, L., Rizzolatti, G., 2014. Space-Dependent Representation of Objects and Other's Action in Monkey Ventral Premotor Grasping Neurons. J. Neurosci. 34, 4108–4119. https://doi.org/10.1523/JNEUROSCI.4187-13.2014.

Borra, E., Luppino, G., 2017. Functional anatomy of the macaque tempo-parieto-frontal connectivity. Cortex 97, 306–326. https://doi.org/10.1016/j.cortex.2016.12.007.

Borra, E., Belmalih, A., Calzavara, R., Gerbella, M., Murata, A., Rozzi, S., Luppino, G., 2008. Cortical Connections of the Macaque Anterior Intraparietal (AIP) Area. Cerebr. Cortex 18, 1094–1111. https://doi.org/10.1093/cercor/bhm146.

Borra, E., Gerbella, M., Rozzi, S., Luppino, G., 2017. The macaque lateral grasping network: A neural substrate for generating purposeful hand actions. Neurosci. Biobehav. Rev. 75, 65–90. https://doi.org/10.1016/j.neubiorev.2017.01.017.

Caminiti, R., Borra, E., Visco-Comandini, F., Battaglia-Mayer, A., Averbeck, B.B., Luppino, G., 2017. Computational Architecture of the Parieto-Frontal Network Underlying Cognitive-Motor Control in Monkeys. eneuro 4. ENEURO.0306-16.2017. https://doi.org/10.1523/ENEURO.0306-16.2017.

Cole, D.M., Smith, S.M., Beckmann, C.F., 2010. Advances and pitfalls in the analysis and interpretation of resting-state FMRI data. Front. Syst. Neurosci. 4, 1–15. https://doi.org/10.3389/fnsys.2010.00008.

Coudé, G., Ferrari, P.F., Rodà, F., Maranesi, M., Borelli, E., Veroni, V., Monti, F., Rozzi, S., Fogassi, L., 2011. Neurons controlling voluntary vocalization in the macaque ventral premotor cortex. PLoS One 6, 1–10. https://doi.org/10.1371/journal.pone.0026822.

Damoiseaux, J.S., Greicius, M.D., 2009. Greater than the sum of its parts: a review of studies combining structural connectivity and resting-state functional connectivity. Brain Struct. Funct. 213, 525–533. https://doi.org/10.1007/s00429-009-0208-6.

di Pellegrino, G., Fadiga, L., Fogassi, L., Gallese, V., Rizzolatti, G., 1992. Understanding motor events: a neurophysiological study. Exp. Brain Res. 91, 176–180. https://doi.org/10.1007/BF00230027.

Durand, J.-B., Nelissen, K., Joly, O., Wardak, C., Todd, J.T., Norman, J.F., Janssen, P., Vanduffel, W., Orban, G.A., 2007. Anterior Regions of Monkey Parietal Cortex Process Visual 3D Shape. Neuron 55, 493–505. https://doi.org/10.1016/j.neuron.2007.06.040.

Ekstrom, L.B., Roelfsema, P.R., Arsenault, J.T., Bonmassar, G., Vanduffel, W., 2008. Bottom-Up Dependent Gating of Frontal Signals in Early Visual Cortex. Science 80 (321), 414–417. https://doi.org/10.1126/science.1153276.

Ferrari, P.F., Gallese, V., Rizzolatti, G., Fogassi, L., 2003. Mirror neurons responding to the observation of ingestive and communicative mouth actions in the monkey ventral premotor cortex. Eur. J. Neurosci. 17, 1703–1714. https://doi.org/10.1046/j.1460-9568.2003.02601.x.

Ferrari, P.F., Gerbella, M., Coudé, G., Rozzi, S., 2017. Two different mirror neuron networks: The sensorimotor (hand) and limbic (face) pathways. Neuroscience 358, 300–315. https://doi.org/10.1016/j.neuroscience.2017.06.052.

Fiave, P.A., Sharma, S., Jastorff, J., Nelissen, K., 2018. Investigating common coding of observed and executed actions in the monkey brain using cross-modal multi-variate fMRI classification. Neuroimage 178, 306–317. https://doi.org/10.1016/j.neuroimage.2018.05.043.

Fluet, M.-C., Baumann, M.A., Scherberger, H., 2010. Context-Specific Grasp Movement Representation in Macaque Ventral Premotor Cortex. J. Neurosci. 30, 15175–15184. https://doi.org/10.1523/JNEUROSCI.3343-10.2010.

Fox, M.D., Raichle, M.E., 2007. Spontaneous fluctuations in brain activity observed with functional magnetic resonance imaging. Nat. Rev. Neurosci. 8, 700–711. https://doi.org/10.1038/nrn2201.

Frey, S., Mackey, S., Petrides, M., 2014. Cortico-cortical connections of areas 44 and 45B in the macaque monkey. Brain Lang. 131, 36–55. https://doi.org/10.1016/j.bandl.2013.05.005.

Friston, K.J., Holmes, A.P., Worsley, K.J., Poline, J.-P., Frith, C.D., Frackowiak, R.S.J., 1994. Statistical parametric maps in functional imaging: A general linear approach. Hum. Brain Mapp. 2, 189–210. https://doi.org/10.1002/hbm.460020402.

Gallese, V., Fadiga, L., Fogassi, L., Rizzolatti, G., 1996. Action recognition in the premotor cortex. Brain 119 (Pt 2), 593–609. https://doi.org/10.1093/brain/119.2.593.

Gardner, E.P., 2017. Neural pathways for cognitive command and control of hand movements. Proc. Natl. Acad. Sci. Unit. States Am. 114, 4048–4050. https://doi.org/10.1073/pnas.1702746114.

Gentilucci, M., Fogassi, L., Luppino, G., Matelli, M., Camarda, R., Rizzolatti, G., 1988. Functional organization of inferior area 6 in the macaque monkey. Exp. Brain Res. 71, 475–490. https://doi.org/10.1007/BF00248741.

Gerbella, M., Belmalih, A., Borra, E., Rozzi, S., Luppino, G., 2011. Cortical connections of the anterior (F5a) subdivision of the macaque ventral premotor area F5. Brain Struct. Funct. 216, 43–65. https://doi.org/10.1007/s00429-010-0293-6.

Gerbella, M., Borra, E., Rozzi, S., Luppino, G., 2016. Connections of the macaque Granular Frontal Opercular (GrFO) area: a possible neural substrate for the contribution of limbic inputs for controlling hand and face/mouth actions. Brain Struct. Funct. 221, 59–78. https://doi.org/10.1007/s00429-014-0892-8.

Gharbawie, O.A., Stepniewska, I., Qi, H., Kaas, J.H., 2011. Multiple Parietal-Frontal Pathways Mediate Grasping in Macaque Monkeys. J. Neurosci. 31, 11660–11677. https://doi.org/10.1523/JNEUROSCI.1777-11.2011.

Ghosh, S., Gattera, R., 1995. A Comparison of the Ipsilateral Cortical Projections to the Dorsal and Ventral Subdivisions of the Macaque Premotor Cortex. Somatosens. Mot. Res. 12, 359–378. https://doi.org/10.3109/08990229509093668.

Gothard, K.M., 2014. The amygdalo-motor pathways and the control of facial expressions. Front. Neurosci. 8, 1–7. https://doi.org/10.3389/fnins.2014.00043.

Goulas, A., Stiers, P., Hutchison, R.M., Everling, S., Petrides, M., Margulies, D.S., 2017. Intrinsic functional architecture of the macaque dorsal and ventral lateral frontal cortex. J. Neurophysiol. 117, 1084–1099. https://doi.org/10.1152/jn.00486.2016.

Grandjean, J., Zerbi, V., Balsters, J.H., Wenderoth, N., Rudin, M., 2017. Structural Basis of Large-Scale Functional Connectivity in the Mouse. J. Neurosci. 37, 8092–8101. https://doi.org/10.1523/JNEUROSCI.0438-17.2017.

Gregoriou, G.G., Borra, E., Matelli, M., Luppino, G., 2006. Architectonic organization of the inferior parietal convexity of the macaque monkey. J. Comp. Neurol. 496, 422–451. https://doi.org/10.1002/cne.20933.

Greicius, M.D., Supekar, K., Menon, V., Dougherty, R.F., 2009. Resting-State Functional Connectivity Reflects Structural Connectivity in the Default Mode Network. Cerebr. Cortex 19, 72–78. https://doi.org/10.1093/cercor/bhn059.

Hage, S.R., Nieder, A., 2013. Single neurons in monkey prefrontal cortex encode volitional initiation of vocalizations. Nat. Commun. 4, 2409. https://doi.org/10.1038/ncomms3409.

Hage, S.R., Nieder, A., 2015. Audio-Vocal Interaction in Single Neurons of the Monkey Ventrolateral Prefrontal Cortex. J. Neurosci. 35, 7030–7040. https://doi.org/10.1523/JNEUROSCI.2371-14.2015.

Hepp-Reymond, M.-C., Hüsler, E.J., Maier, M.A., Qi, H.-X., 1994. Force-related neuronal activity in two regions of the primate ventral premotor cortex. Can. J. Physiol. Pharmacol. 72, 571–579. https://doi.org/10.1139/y94-081.

Honey, C.J., Sporns, O., Cammoun, L., Gigandet, X., Thiran, J.P., Meuli, R., Hagmann, P., 2009. Predicting human resting-state functional connectivity from structural connectivity. Proc. Natl. Acad. Sci. Unit. States Am. 106, 2035–2040. https://doi.org/10.1073/pnas.0811168106.

Huang, C.S., Sirisko, M. a, Hiraba, H., Murray, G.M., Sessle, B.J., 1988. Organization of the primate face motor cortex as revealed by intracortical microstimulation and electrophysiological identification of afferent inputs and corticobulbar projections. J. Neurophysiol. 59, 796–818. https://doi.org/10.1152/jn.1988.59.3.796.

Hutchison, R.M., Leung, L.S., Mirsattari, S.M., Gati, J.S., Menon, R.S., Everling, S., 2011. Resting-state networks in the macaque at 7T. Neuroimage 56, 1546–1555. https://doi.org/10.1016/j.neuroimage.2011.02.063.

Hutchison, R.M., Gallivan, J.P., Culham, J.C., Gati, J.S., Menon, R.S., Everling, S., 2012. Functional connectivity of the frontal eye fields in humans and macaque monkeys investigated with resting-state fMRI. J. Neurophysiol. 107, 2463–2474. https://doi.org/10.1152/jn.00891.2011.

Hutchison, R.M., Culham, J.C., Flanagan, J.R., Everling, S., Gallivan, J.P., 2015. Functional subdivisions of medial parieto-occipital cortex in humans and nonhuman primates using resting-state fMRI. Neuroimage 116, 10–29. https://doi.org/10.1016/j.neuroimage.2015.04.068.

Ishida, H., Fornia, L., Grandi, L.C., Umiltà, M.A., Gallese, V., 2013. Somato-Motor Haptic Processing in Posterior Inner Perisylvian Region (SII/pIC) of the Macaque Monkey. PLoS One 8, e69931. https://doi.org/10.1371/journal.pone.0069931.

Jeannerod, M., Arbib, M.A., Rizzolatti, Gl., Sakata, H., 1995. Grasping objects: the cortical mechanisms of visuomotor transformation. Trends Neurosci. 18, 314–320. https://doi.org/10.1016/0166-2236(95)93921-J.

Jezzini, A., Caruana, F., Stoianov, I., Gallese, V., Rizzolatti, G., 2012. Functional organization of the insula and inner perisylvian regions. Proc. Natl. Acad. Sci. Unit. States Am. 109, 10077–10082. https://doi.org/10.1073/pnas.1200143109.

Joly, O., Vanduffel, W., Orban, G.A., 2009. The monkey ventral premotor cortex processes 3D shape from disparity. Neuroimage 47, 262–272. https://doi.org/10.1016/j.neuroimage.2009.04.043.

Kaskan, P.M., Dean, A.M., Nicholas, M.A., Mitz, A.R., Murray, E.A., 2019. Gustatory responses in macaque monkeys revealed with fMRI: Comments on taste, taste preference, and internal state. Neuroimage 184, 932–942. https://doi.org/10.1016/j.neuroimage.2018.10.005.

Kolster, H., Mandeville, J.B., Arsenault, J.T., Ekstrom, L.B., Wald, L.L., Vanduffel, W., 2009. Visual Field Map Clusters in Macaque Extrastriate Visual Cortex. J. Neurosci. 29, 7031–7039. https://doi.org/10.1523/JNEUROSCI.0518-09.2009.

Kraskov, A., Dancause, N., Quallo, M.M., Shepherd, S., Lemon, R.N., 2009. Corticospinal Neurons in Macaque Ventral Premotor Cortex with Mirror Properties: A Potential Mechanism for Action Suppression? Neuron 64, 922–930. https://doi.org/10.1016/j.neuron.2009.12.010.

Krubitzer, L., Clarey, J., Tweedale, R., Elston, G., Calford, M., 1995. A redefinition of somatosensory areas in the lateral sulcus of macaque monkeys. J. Neurosci. 15, 3821–3839. https://doi.org/10.1523/JNEUROSCI.15-05-03821.1995.

Kurata, K., 1991. Corticocortical inputs to the dorsal and ventral aspects of the premotor cortex of macaque monkeys. Neurosci. Res. 12, 263–280. https://doi.org/10.1016/0168-0102(91)90116-G.

Kurata, K., 2018. Hierarchical Organization Within the Ventral Premotor Cortex of the Macaque Monkey. Neuroscience 382, 127–143. https://doi.org/10.1016/j.neuroscience.2018.04.033.

Kurata, K., Tanji, J., 1986. Premotor cortex neurons in macaques: activity before distal and proximal forelimb movements. J. Neurosci. 6, 403–411. https://doi.org/10.1523/JNEUROSCI.06-02-00403.1986.

Mandeville, J.B., Marota, J.J.A., Ayata, C., Zaharchuk, G., Moskowitz, M.A., Rosen, B.R., Weisskoff, R.M., 1999. Evidence of a Cerebrovascular Postarteriole Windkessel With Delayed Compliance. J. Cerebr. Blood Flow Metabol. 679–689. https://doi.org/10.1097/00004647-199906000-00012.

Mantini, D., Gerits, A., Nelissen, K., Durand, J.-B., Joly, O., Simone, L., Sawamura, H., Wardak, C., Orban, G.A., Buckner, R.L., Vanduffel, W., 2011. Default Mode of Brain Function in Monkeys. J. Neurosci. 31, 12954–12962. https://doi.org/10.1523/JNEUROSCI.2318-11.2011.

Maranesi, M., Rodà, F., Bonini, L., Rozzi, S., Ferrari, P.F., Fogassi, L., Coudé, G., 2012. Anatomo-functional organization of the ventral primary motor and premotor cortex in the macaque monkey. Eur. J. Neurosci. 36, 3376–3387. https://doi.org/10.1111/j.1460-9568.2012.08252.x.

Margulies, D.S., Vincent, J.L., Kelly, C., Lohmann, G., Uddin, L.Q., Biswal, B.B., Villringer, A., Castellanos, F.X., Milham, M.P., Petrides, M., 2009. Precuneus shares intrinsic functional architecture in humans and monkeys. Proc. Natl. Acad. Sci. Unit. States Am. 106, 20069–20074. https://doi.org/10.1073/pnas.0905314106.

Matelli, M., Luppino, G., Rizzolatti, G., 1985. Patterns of cytochrome oxidase activity in the frontal agranular cortex of the macaque monkey. Behav. Brain Res. 18, 125–136. https://doi.org/10.1016/0166-4328(85)90068-3.

Matelli, M., Camarda, R., Glickstein, M., Rizzolatti, G., 1986. Afferent and efferent projections of the inferior area 6 in the macaque monkey. J. Comp. Neurol. 251, 281–298. https://doi.org/10.1002/cne.902510302.

Matelli, M., Govoni, P., Galletti, C., Kutz, D.F., Luppino, G., 1998. Superior area 6 afferents from the superior parietal lobule in the macaque monkey. J. Comp. Neurol. 402, 327–352. https://doi.org/10.1002/(SICI)1096-9861(19981221)402:3<327::AID-CNE4>3.0.CO;2-Z.

Miranda-Dominguez, O., Mills, B.D., Grayson, D., Woodall, A., Grant, K.A., Kroenke, C.D., Fair, D.A., 2014. Bridging the Gap between the Human and Macaque Connectome: A Quantitative Comparison of Global Interspecies Structure-Function Relationships and Network Topology. J. Neurosci. 34, 5552–5563. https://doi.org/10.1523/JNEUROSCI.4229-13.2014.

Morecraft, R.J., Stilwell-Morecraft, K.S., Rossing, W.R., 2004. The Motor Cortex and Facial Expression: Neurologist, vol. 10, pp. 235–249. https://doi.org/10.1097/01.nrl.0000138734.45742.8d.

Murata, A., Fadiga, L., Fogassi, L., Gallese, V., Raos, V., Rizzolatti, G., 1997. Object Representation in the Ventral Premotor Cortex (Area F5) of the Monkey. J. Neurophysiol. 78, 2226–2230. https://doi.org/10.1152/jn.1997.78.4.2226.

Murata, A., Gallese, V., Luppino, G., Kaseda, M., Sakata, H., 2000. Selectivity for the Shape, Size, and Orientation of Objects for Grasping in Neurons of Monkey Parietal Area AIP. J. Neurophysiol. 83, 2580–2601. https://doi.org/10.1152/jn.2000.83.5.2580.

Murray, G.M., Sessle, B.J., 1992. Functional properties of single neurons in the face primary motor cortex of the primate. II. Relations with trained orofacial motor behavior. J. Neurophysiol. 67, 759–774. https://doi.org/10.1152/jn.1992.67.3.759.

Nelissen, K., Luppino, G., Vanduffel, W., Rizzolatti, G., Orban, G.A., 2005. Observing Others: Multiple Action Representation in the Frontal Lobe. Science 80 (310), 332–336. https://doi.org/10.1126/science.1115593.

Nelissen, K., Vanduffel, W., 2011. Grasping-related functional magnetic resonance imaging brain responses in the macaque monkey. J. Neurosci. 31, 8220–8229. https://doi.org/10.1523/JNEUROSCI.0623-11.2011.

Nelissen, K., Fiave, P.A., Vanduffel, W., 2018. Decoding Grasping Movements from the Parieto-Frontal Reaching Circuit in the Nonhuman Primate. Cerebr. Cortex 28, 1245–1259. https://doi.org/10.1093/cercor/bhx037.

Nelson, R.J., Sur, M., Felleman, D.J., Kaas, J.H., 1980. Representations of the body surface in postcentral parietal cortex of Macaca fascicularis. J. Comp. Neurol. 192, 611–643. https://doi.org/10.1002/cne.901920402.

Neubert, F.-X., Mars, R.B., Thomas, A.G., Sallet, J., Rushworth, M.F.S., 2014. Comparison of Human Ventral Frontal Cortex Areas for Cognitive Control and Language with Areas in Monkey Frontal Cortex. Neuron 81, 700–713. https://doi.org/https://doi.org/10.1016/j.neuron.2013.11.012.

Nieder, A., 2018. Primate Social Communication Goes Interactive. Neuron 99, 250–253. https://doi.org/10.1016/j.neuron.2018.07.014.

Ogawa, H., 1994. Gustatory cortex of primates: anatomy and physiology. Neurosci. Res. 20, 1–13. https://doi.org/10.1016/0168-0102(94)90017-5.

Ogawa, H., Ito, S.-I., Nomura, T., 1989. Oral cavity representation at the frontal operculum of macaque monkeys. Neurosci. Res. 6, 283–298. https://doi.org/10.1016/0168-0102(89)90021-7.

Palomero-Gallagher, N., Zilles, K., 2018. Differences in cytoarchitecture of Broca's region between human, ape and macaque brains. Cortex 1–22. https://doi.org/10.1016/j.cortex.2018.09.008.

Petrides, M., Cadoret, G., Mackey, S., 2005. Orofacial somatomotor responses in the macaque monkey homologue of Broca's area. Nature 435, 1235–1238. https://doi.org/10.1038/nature03628.

Petrides, M., Pandya, D.N., 1994. Comparative architectonic analysis of the human and the macaque frontal cortex. In: Boller, F., Grafman, J. (Eds.), Handb. Neuropsychol. Amsterdam. Elsevier, pp. 17–58.

Premereur, E., Van Dromme, I.C., Romero, M.C., Vanduffel, W., Janssen, P., 2015. Effective Connectivity of Depth-Structure–Selective Patches in the Lateral Bank of the Macaque Intraparietal Sulcus. PLoS Biol. 13, e1002072. https://doi.org/10.1371/journal.pbio.1002072.

Preuss, T.M., Goldman-Rakic, P.S., 1991. Myelo- and cytoarchitecture of the granular frontal cortex and surrounding regions in the strepsirhine primateGalago and the anthropoid primateMacaca. J. Comp. Neurol. 310, 429–474. https://doi.org/10.1002/cne.903100402.

Qi, H.-X., Preuss, T.M., Kaas, J.H., 2008. Somatosensory areas of the cerebral cortex: architectonic characteristics and modular organization.

Raos, V., Umiltá, M.-A., Murata, A., Fogassi, L., Gallese, V., 2006. Functional Properties of Grasping-Related Neurons in the Ventral Premotor Area F5 of the Macaque Monkey. J. Neurophysiol. 95, 709–729. https://doi.org/10.1152/jn.00463.2005.

Rizzolatti, G., Luppino, G., 2001. The cortical motor system. Neuron 31, 889–901. https://doi.org/10.1016/S0896-6273(01)00423-8.

Rizzolatti, G., Camarda, R., Fogassi, L., Gentilucci, M., Luppino, G., Matelli, M., 1988. Functional organization of inferior area 6 in the macaque monkey. Exp. Brain Res. 71, 491–507. https://doi.org/10.1007/BF00248742.

Rolls, E.T., 2015. Taste, olfactory, and food reward value processing in the brain. Prog. Neurobiol. 127–128, 64–90. https://doi.org/10.1016/j.pneurobio.2015.03.002.

Rolls, E.T., Yaxley, S., Sienkiewicz, Z.J., 1990. Gustatory responses of single neurons in the caudolateral orbitofrontal cortex of the macaque monkey. J. Neurophysiol. 64, 1055–1066. https://doi.org/10.1152/jn.1990.64.4.1055.

Rozzi, S., Ferrari, P.F., Bonini, L., Rizzolatti, G., Fogassi, L., 2008. Functional organization of inferior parietal lobule convexity in the macaque monkey: electrophysiological characterization of motor, sensory and mirror responses and their correlation with cytoarchitectonic areas. Eur. J. Neurosci. 28, 1569–1588. https://doi.org/10.1111/j.1460-9568.2008.06395.x.

Schaffelhofer, S., Scherberger, H., 2016. Object vision to hand action in macaque parietal, premotor, and motor cortices. Elife 5, 1–24. https://doi.org/10.7554/eLife.15278.

Scott, T.R., Yaxley, S., Sienkiewicz, Z.J., Rolls, E.T., 1986. Gustatory responses in the frontal opercular cortex of the alert cynomolgus monkey. J. Neurophysiol. 56, 876–890. https://doi.org/10.1152/jn.1986.56.3.876.

Sharma, S., Fiave, P.A., Nelissen, K., 2018. Functional MRI Responses to Passive, Active, and Observed Touch in Somatosensory and Insular Cortices of the Macaque Monkey. J. Neurosci. 38, 3689–3707. https://doi.org/10.1523/JNEUROSCI.1587-17.2018.

Shen, K., Bezgin, G., Hutchison, R.M., Gati, J.S., Menon, R.S., Everling, S., McIntosh, A.R., 2012. Information Processing Architecture of Functionally Defined Clusters in the Macaque Cortex. J. Neurosci. 32, 17465–17476. https://doi.org/10.1523/JNEUROSCI.2709-12.2012.

Shepherd, S.V., Freiwald, W.A., 2018. Functional Networks for Social Communication in the Macaque Monkey. Neuron 99, 413–420 e3. https://doi.org/10.1016/j.neuron.2018.06.027.

Squatrito, S., Raffi, M., Maioli, M.G., Battaglia-Mayer, A., 2001. Visual Motion Responses of Neurons in the Caudal Area PE of Macaque Monkeys. J. Neurosci. 21. RC130-RC130. https://doi.org/10.1523/JNEUROSCI.21-04-j0002.2001.

Takahashi, K., Best, M.D., Huh, N., Brown, K.A., Tobaa, A.A., Hatsopoulos, N.G., 2017. Encoding of Both Reaching and Grasping Kinematics in Dorsal and Ventral Premotor Cortices. J. Neurosci. 37, 1733–1746. https://doi.org/10.1523/JNEUROSCI.1537-16.2016.

Theys, T., Pani, P., van Loon, J., Goffin, J., Janssen, P., 2012. Selectivity for Three-Dimensional Shape and Grasping-Related Activity in the Macaque Ventral Premotor Cortex. J. Neurosci. 32, 12038–12050. https://doi.org/10.1523/JNEUROSCI.1790-12.2012.

Touroutoglou, A., Bliss-Moreau, E., Zhang, J., Mantini, D., Vanduffel, W., Dickerson, B.C., Barrett, L.F., 2016. A ventral salience network in the macaque brain. Neuroimage 132, 190–197. https://doi.org/10.1016/j.neuroimage.2016.02.029.

Vogt, O., Vogt, C., 1919. Allgemeinere Ergebnisse unserer Hirnforschung. J. Psychol. Neurol. 25, 279–462.

van den Heuvel, M.P., Hulshoff Pol, H.E., 2010. Specific somatotopic organization of functional connections of the primary motor network during resting state. Hum. Brain Mapp. 31, 631–644. https://doi.org/10.1002/hbm.20893.

Vanduffel, W., Fize, D., Mandeville, J.B., Nelissen, K., Van Hecke, P., Rosen, B.R., Tootell, R.B., Orban, G.A., 2001. Visual Motion Processing Investigated Using Contrast Agent-Enhanced fMRI in Awake Behaving Monkeys. Neuron 32, 565–577. https://doi.org/10.1016/S0896-6273(01)00502-5.

Vijayakumar, S., Sallet, J., Verhagen, L., Folloni, D., Medendorp, W.P., Mars, R.B., 2018. Mapping multiple principles of parietal–frontal cortical organization using functional connectivity. Brain Struct. Funct. 0, 0. https://doi.org/10.1007/s00429-018-1791-1.

Vincent, J.L., Patel, G.H., Fox, M.D., Snyder, A.Z., Baker, J.T., Van Essen, D.C., Zempel, J.M., Snyder, L.H., Corbetta, M., Raichle, M.E., 2007. Intrinsic functional architecture in the anaesthetized monkey brain. Nature 447, 83–86. https://doi.org/10.1038/nature05758.

Vogt, B.A., 2009. Regions and Subregions of the Cingulate Cortex Cytological Regions. In: Vogt, B.A. (Ed.), Cingulate neubiology and disease. Oxford University Press, pp. 3–30.

von Bonin, G., Bailey, P., 1947. The neocortex of Macaca mulatta. Univ. Illinois Press, Urbana, p. 136.

Wang, Z., Chen, L.M., Négyessy, L., Friedman, R.M., Mishra, A., Gore, J.C., Roe, A.W., 2013. The Relationship of Anatomical and Functional Connectivity to Resting-State Connectivity in Primate Somatosensory Cortex. Neuron 78, 1116–1126. https://doi.org/10.1016/j.neuron.2013.04.023.

Yaxley, S., Rolls, E.T., Sienkiewicz, Z.J., 1990. Gustatory responses of single neurons in the insula of the macaque monkey. J. Neurophysiol. 63, 689–700. https://doi.org/10.1152/jn.1990.63.4.689.